CHARACTERIZATION OF Ni-BASED METALLIC GLASS IN A CRYSTALLINE-AMORPHOUS COMPOSITE SYNTHESIZED BY ACCUMULATIVE ROLL BONDING

BY

TAIWO OLUWATOYIN DADA

A thesis submitted to the faculty of Graduate Studies of the University of Manitoba in partial fulfillment of the requirements for the degree of

MASTER OF SCIENCE

Department of Mechanical Engineering,

University of Manitoba. Winnipeg

Canada

Acknowledgement

My deepest appreciation goes to my awesome supervisors: Dr. Chuang Deng and Dr. Olanrewaju Ojo. I am grateful for their patience, guidance, steady support, words of encouragement and amazing ideas towards the completion of this research. I would also like to appreciate our amazing laboratory technician, Trevor, who was always ready to help.

I would also like to thank my colleagues, and former colleagues in my research group: Afzal Neelav, Ehsan Alishahi, Mohammed Aramfard, Navjot Kaur, and Farhad. My appreciation also goes out to my team of extraordinary friends: Olaitan Lawal, Samuel Osho, Rotimi Ajigboye, David Nwankwo, Tobi Mutiu, Emmanuel Adejumo, Emeka Ugodilinwa, Gbenga Asala, Francis Amushi, Chidinma Anyanwu, Dr. Osoba, Dr. Lina, Ibrahim Abdulganiyu, Sanmi Oguntuase, James Adu, Oluyemi Aina, Ebun Micheal, Nengie George, Dupe Oripeloye, Funke, Jamiu, and Bolu Hassan.

This research would have been impossible without the unconditional love and support of my family; kudos to my amazing parents and kind siblings.

Finally and most importantly, thanks to the almighty God for wisdom, strength and the ability to complete my program successfully.

Dedication

I dedicate this master's thesis to

The Almighty God for guiding and leading through everything. I also dedicate this thesis to my awesome mother who has always been there for me

List of Acronyms

List of Acronyms	Description
BMG	Bulk Metallic Glass
MG	Metallic Glass
C-A	Crystalline-Amorphous
ARB	Accumulative Roll Bonding
SEM	Scanning Electron Microscope
OM	Optical Microscope
EDS	Electron-Dispersive X-ray Spectroscopy
STZ	Shear Transformation Zone
XRD	X-ray Diffraction
d_{hkl}	Inter-planer Spacing
T_g	Glass Transition Temperature
T_m	Melting Temperature
FIB	Focused Ion Beam

Abstract

Bulk metallic glasses are known for their ultra-high strength but little or no plasticity. Synthesizing crystalline-amorphous (C-A) composites presents a way by which the plasticity can be improved. In the present study, Accumulative Roll Bonding (ARB) is used to process a composite of copper/nickel and a nickel-based metallic glass up to four cycles without heat treatment. While the effects of ARB have been well documented for crystalline materials, not much has been done for amorphous materials. Current research aimed to use the ARB technique to synthesize a crystalline-amorphous (C-A) composite and characterise the amorphous phase using optical microscopy (OM), scanning electron microscopy (SEM), differential scanning calorimetry (DSC) and nanoindentation. By using OM, rupture of the hard metallic glass phase was detected after one cycle. The C-A sheets deformed inhomogeneously, accompanied by the formation of multiple fractures of the MG layers. Further ARB passes showed that the metallic glass fragments were broken into smaller pieces and distributed more homogeneously in the crystalline matrix. Although DSC studies showed no change in the crystallization temperature after the fourth ARB cycle, nanoindentation studies revealed an increase of 11.34% in the hardness of the MG after the fourth ARB cycle and a 16.06% increase in the hardness of the MG due to annealing at 400 ^{o}C. The same trend was observed with the elastic modulus of the metallic glass as there was a property increase due to strain application and annealing temperature. However, no size effect was observed.

Table of Contents

List of Figures

List of Tables

Chapter 1 - Introduction

1.1 Background Information

Bulk metallic glasses have attracted a lot of attention due to their ultra-high strength and hardness [1]–[3]. They exhibit a unique combination of mechanical, chemical, and physical properties. It is for this reason that they have great potentials to be used in several applications such as cutting materials, corrosion resistant materials, hydrogen storage materials, ornamental materials, machinery structural materials and so on [1]–[3]. They are amorphous in nature which means that they do not possess a long-range order of arrangement atoms like the crystalline metals. More so, they do not possess crystalline defects like vacancies, dislocations and grain boundaries. These metallic glasses are formed by cooling a melt of a particular composition at a very high cooling rate. This way, the atoms do not have enough time to relax and form a long-range order.

Despite the awesome properties displayed by metallic glasses, they exhibit low or no plasticity at room temperature. This is because they deform inhomogeneously by forming localized shear bands without exhibiting any strain hardening as compared to crystalline metals [4]. As plasticity in crystalline metals is governed by the movement of dislocation, the onset of plastic deformation in bulk metallic glasses (BMGs) takes place by the formation of a shear band. Once this shear band is formed, it propagates rapidly, leading to fracture of the metallic glass. Metallic glasses can fail due to the formation of just one shear band. Therefore, for engineering and industrial applications, the plasticity of the BMGs has to be enhanced and this can be achieved by promoting the formation of multiple shear bands.

Previous research has shown that the plasticity of BMGs can be improved by introducing crystalline phases in the metallic glass matrix [5]. These crystalline phases increase the number of shear bands formed in the material. The crystalline materials act as blockades, impeding the movement of the shear bands. This results in shear bands forming in other parts of the material. Therefore, more research has been put into synthesizing crystalline-amorphous composites. Melting and Quenching [6], Sputtering [7] and Accumulative Roll Bonding (ARB) [8] are ways to synthesize these composites. While the first two methods are effective in fabricating the composites, they have some limitations which include limited sample size and complexities in developing the composites.

ARB, on the other hand, has the capacity to synthesize a large sample size. It involves making a sandwich of desired materials, stacking them, and rolling them to the desired thickness (usually >50%), cutting and then repeating the process all over again. It is a rolling process as well as a bonding process. In this research, the concept of ARB was used to develop a crystalline-amorphous composite with the amorphous materials being dispersed in the crystalline matrix. The mechanical properties of composites are highly dependent on the reinforcing materials. In this case, the reinforcing material is metallic glass.

In order to design and characterize C-A composites processed by ARB, it is important to characterise the structure and mechanical properties of each phase and their dependence on processing strain, temperature, and their microstructure (sample size). While this dependence has been extensive studied and documented for crystalline metals, which include strain hardening, size effects, recrystallization, recovery and grain growth, limited work has been done for amorphous materials. Therefore, a model system was chosen based on a Ni-based metallic glass and crystalline Cu/Ni to explore this topic.

Optical microscopy and scanning electron microscopy were used to study the microstructural evolution of the C-A system after each pass and to study the bonding at the interface between the bonded materials. DSC was used to study the crystallization temperature of the amorphous material and nanoindentation was used to investigate the hardness and elastic modulus properties of the amorphous material. Nanoindentation is a complex technique used by researchers to determine mostly the hardness and elastic modulus of materials even when they are very small. This research made use of this sophisticated tool to characterize the hardness and modulus of submicron metallic glass particles in the crystalline matrix. Load-displacement curves are plotted during the loading and unloading cycle and the hardness and modulus are calculated from these curves.

1.2 Research Objectives

The objectives of this research are:

1. To develop a crystalline-amorphous composite by ARB.
2. To study the effect of ARB parameters on the properties of metallic glass.
3. To study the effect of size on the hardness and elastic modulus of the metallic glass.

1.3 Thesis Structure

- Chapter 1 presents the introduction which covers the background information, research objectives, major findings, and thesis structure.
- Chapter 2 presents a literature review on the structure and properties of crystalline metals and amorphous metals. It also provides an overview of crystalline-amorphous composites and how they are synthesized. In addition, the concept of ARB is reviewed as well as the process involved in nanoindentation.
- Chapter 3 presents the materials and metallographic equipment used for the analysis of this study. It also contains detailed sample preparation and mechanical characterization using nanoindentation.
- Chapter 4 presents the microstructural evolution of the Cu/MG system, followed up by discussions. It also presents the results from nanoindentation regarding the effect of strain, heat treatment and size of the metallic glass. In addition, the results from the heat treatment of the Ni/MG and Cu/MG system above the crystallization temperature of the metallic glass was discussed.
- Finally, the summary and conclusions of this research work, accompanied by the future work and recommendations are contained in Chapter 5.

Chapter 2 - Literature Review

2.1 Crystalline Metals

The arrangement of their atoms comes into play in the classification of solid materials. When atoms are arranged in such a way that they are in a recurring or periodic array; the material is termed a “crystalline material”. In other words, the atoms possess a long-range order, so that when they solidify, these atoms will arrange themselves in a recurring 3-D pattern, such that each atom is bonded to its nearest adjacent atoms. It is important to note that all metals possess this crystalline structure under normal solidification conditions.

The crystal structure of a material determines some of its properties. Sub-diving crystal structures into unit cells is a convenient way of describing crystal structures [9]. The unit cells are small repeat entities which could be parallelepipeds or prisms. There exist three simple crystal structures in most metals. These crystal structures include: the face-centered cubic (FCC), the body-centered cubic (BCC) and the hexagonal close-packed (HCP). Metals like copper and aluminum possess the FCC crystal structure. This structure has a cubic geometry. The atoms are arranged in such a way that they exist at each corner and faces of the cube. Unlike the FCC structure, the BCC structure is arranged such that each of its corners are contained by an atom and a singular atom in the center of the cube. Metals like chromium and iron exhibit this BCC structure. The HCP structure, on the other hand, is not cubic as the name implies. The unit cell of the structure is hexagonal with the top and bottom faces having atoms on each corner surrounding an atom in the center. Metals that exhibit this structure are cadmium, magnesium, titanium and so on.

The structure of crystalline solids can be determined using the X-ray diffraction method. It is the most popular technique used to deduce crystal structures. X-rays are emitted through an

electromagnetic radiation source. These X-rays have very high energies and short wavelength [10]. Some of the emitted X-ray beams is then scattered by the crystalline inter-planer spacing (d_{hkl}) at an angle of diffraction (θ). Bragg's law is then used to show the relationship between X-ray wavelength (λ), d_{hkl} and θ. This law is illustrated with the equation below:

$$n\lambda = 2d_{hkl} \sin\theta \qquad \text{Equation 2-1}$$

The diffraction pattern is then plotted as diffraction intensity against diffraction angle (2θ). Discrete peaks will then appear on the pattern depending on the crystal structure and nearest neighbouring atoms.

Crystalline materials are accompanied by crystalline defects which are a deviation from the perfect order of arrangement throughout the crystalline material. These defects include vacancies and self-interstitials which are point defects, dislocations which are linear defects, area defects such as grain boundaries, twin boundaries, stacking faults, and phase boundaries and volume defects such as pores and cracks [9]. These defects constitute plastic deformation in these materials.

Under applied stress beyond the yield stress, deformation in crystalline materials is governed by the movement of a large number of dislocations [9]. This phenomenon in which dislocation motion causes plastic deformation is termed as "slip". Dislocations move in preferred planes and directions called the slip planes and slip directions respectively. The association of these two is called the slip system. The slip plane is the plane that has the largest number of atoms for a particular crystal structure. For FCC crystal structure, for example, has a {111}<110> slip system which represents both the slip plane and the slip direction.

2.1.1 Mechanical Properties of Crystalline Metals

The mechanical properties discussed in this section are properties associated with strain hardening, the effect of heat treatment and size effect.

2.1.1.1 Strain Hardening in Crystalline Metals

When ductile metals are plastically deformed, they become harder and stronger. This phenomenon is called strain hardening or work hardening. Most metals exhibit this phenomenon at room temperature. Due to plastic deformation, dislocation density in the metal increases. The distance between each dislocation then decreases giving rise to dislocations positioned very close to each other. There is a strong repulsive force between dislocation-dislocation strain interactions in such a way that the movement of dislocation is obstructed by the existence of other dislocations. As dislocation multiplies, the obstruction to the movement of dislocation also increases. Therefore, more force is required to further deform the material. This is the basic concept of strain hardening.

This phenomenon is widely used by industries during fabrication, to improve the mechanical properties of metals. The effects of cold working can be eliminated by heating the metal at elevated temperatures which are described in section 2.1.1.2 below.

2.1.1.2 Effect of Heat Treatment on Crystalline Metals

The plastic deformation of polycrystalline materials results in some changes in the mechanical and microstructural properties. These properties include the shape of the grains, work hardening and an obvious increase in the number of dislocations present as discussed in section 2.1.1.1. Also, some of the energy disbursed during deformation remains in the metal and serves as strain energy. During heat treatment, these properties described above may go back to the pre-worked states. Recovery, recrystallization and grain growth are the processes that occur during heat treatment.

During the recovery stage, part of the stored energy caused by strain is alleviated, due to diffusion of atoms at high temperatures. The amount of dislocation also decreases giving rise to lower strain energies.

Even after recovery, the grains still remain in a somewhat high strain energy state. Recrystallization is when new sets of grains are formed, identical to the pre-cold worked condition, free from strain, and with crystals having axes of approximately the same length. These new grains have approximately equal dimensions in all directions. This phenomenon is due to the disparity in the internal energies between the deformed and un-deformed material. During recrystallization, there is a restoration of the mechanical properties that was changed due to cold working.

As heat treatment proceeds, on completion of the recrystallization phase, the newly formed grains, free of strain will continue to grow. This phenomenon is called grain growth. As the size of the grain increases, it leads to a reduction in the total boundary area, giving rise to a reduction in the total energy.

For most polycrystalline metals, the diameter of the grain *d* varies with time *t* in relation to the equation:

$$d^n - d_0^n = Kt \qquad \text{Equation 2-2}$$

Where d_0 is the initial diameter of the grain at t = 0, and K and n are time-dependent constants.

2.1.1.3 Size Effect

Metals and alloys exist mainly in polycrystalline form, therefore, plastic deformation involves the interaction between grain boundaries and dislocations. When in bulk form, the grain boundaries act as hindrance to the movement of dislocation as explained by the Hall-Petch relation depicting an increase in the yield stress of polycrystalline materials with reducing obstacle distance. This

relation is valid for grain sizes of about 40 nm and above [11]–[13]. These grains however, cannot accommodate multiple lattice dislocations when their sizes are reduced below 40 nm. This leads to different plastic deformation phenomena such as sliding of grain-boundary, partial dislocation emission and absorption at grain boundaries [14]–[19]. Most of these special phenomena were observed through deformation of very thin film, where the combination of outer dimensions and nanocrystalline microstructure play a role. For example, Gianola et al. tested nanocrystalline Al films and observed improved plasticity during tension of the sub-micron thick sample. This attributed this observation to stress-induced grain growth and stress-coupled grain boundary migration [18]–[20].

Several research groups have studied size effects in various crystalline metals. These studies have ranged from pure singles crystals like Cu [21], [22], Au [23], [24] and Al [25], [26] to superalloys [27], [28] and have recorded changes in flow strength as the size of the particles decrease. Jang and Greer [29] performed uniaxial tension and compression experiment on Ni-W nano-pillars and observed that their strength reduced by 42% when compared to bulk sizes. Rinaldi et al. [30] also performed size effect experiments on Ni nano-pillars and observed improved properties as the size decreased.

Since single crystals do not possess grain boundaries, size effects due to grain boundary sliding and grain boundary absorption do not come into play. On the other hand, some researchers have proposed “hardening by dislocation starvation”, where pre-existing or newly generated mobile dislocations escape the sample at the free surface faster than they multiply [31], [32].

The most widely used approach to measuring sample size effects is the focused ion beam (FIB) approach [33], [34]. FIB is used to produce micromechanical test specimens. These specimens can then be tested using high resolution loading like a nanoindenter. A simple and straight-forward

experiment involves uniaxial compression of FIB-machined specimens using a nanoindenter outfitted with a flat punch.

2.2 Amorphous Metals

Amorphous metals, unlike crystalline materials, are materials that do not possess the long-range order of arrangement of atoms. These materials do not have grains, neither do they possess crystalline defects like dislocation and grain boundaries. They are formed by heating a material to a very high temperature and then quenching with very high cooling rate. Amorphous materials are on numerous occasions referred to as super cooled or high viscosity liquids, even though they are solids. Another unique feature of amorphous materials is the nonexistence of noticeable discontinuity in their properties when the liquid cools down and becomes a glass. This, however, distinguishes them from crystalline materials, which experience a well-defined transition from liquid to solid as the temperature decreases to below the melting temperature (T_m).

The phenomenon by which a liquid solidifies to form glass involves a step by step process compared to crystalline solid, and this is often called glass transition. During the process of glass transition, the slope of properties, such as density, exhibits a noticeable change with a decrease in temperature. The glass-transition temperature, T_g, occurs over a span of temperatures and is most times described as the mid-point of this span. The glass transition temperature is not distinctively defined, however, it depends on the cooling rate of the liquid. This is in contrast to the clear transformation temperatures in crystalline solids such as boiling and freezing points. Typically, as cooling rate reduces, the glass transition temperature also reduces.

Amorphous solids, also known as glassy alloys or metallic glass possess amazing properties because while in their compact structure, the movement of atoms at room temperature is blocked

by barriers caused by potential energy. During stress-induced deformation, metallic glasses absorb less energy than their crystalline counterparts, and with no defects like dislocation, their mechanical properties blend to produce remarkable high strength material [35].

2.2.1 Plastic Deformation in Amorphous Metals

Over the years, quite a number of bulk metallic glasses with different compositions and base metals such as Ni- [36]. Y-, Zr- [37], [38], Pd- [39], [40], Co- [41], Ca- [42], Cu- [43], Au- [44], La- [45], Fe- [46], Mg- [47], Ti- [48], Hf- [49], Ce-based [50], have been discovered, with sizes up to centimetre or even inch scale. In comparison to crystalline materials, BMGs possess extremely high strength with no dislocations. When stress is applied to amorphous materials, these materials allow little displacement of atoms to resist deformation. Plastic deformation in metallic glasses is controlled by both normal and shear stresses. This deformation is inhomogeneous as a result of concentrated plastic strains in localized shear bands. However, at elevated temperatures and low applied stresses, they exhibit stable Newtonian flow [51]. Lund and Schuh [52] summarised the macroscopic yield and fracture of metallic glass. The deformation consists of many small-scale activities including:

i. Initiation of shear transformation zones (STZs) in which a group of atoms rearranges themselves as a result of the applied shear strain,
ii. Increase in shear localization or growth of the shear bands [53],
iii. Adiabatic heating in those localized deformed regions [54],
iv. Evolution of nanocrystals in the shear bands or close to the shear bands [54],
v. Evolution of very small voids in shear bands, typically in the nanoscale [55],
vi. Fusion of these voids resulting in final failure [56].

Various theories have been proposed explaining the plastic behaviour of metallic glasses. At the atomic level, when stress is applied, there is a local reordering of atoms around the region of free volume to accommodate this stress. This local reordering theory was presented by Argon [4]. It considered two modes of thermally-activated shear transformation processes. The transformation takes place in STZs, somewhat similar to the formation of dislocation loop. The underlying reason for plasticity in metallic glasses can be either STZ or the free volume for atomic jumps. The STZ is a small mass of atoms that are closely packed. When stress is applied, the small mass of atoms rearranges themselves to accommodate the applied strain [52], as shown schematically in figure 2.1 [4]. As the applied strain continues, the STZs also continue to increases until they reach a critical point and large planar bands of STZs or "shear bands" are formed. Metallic glasses fail due to the propagation of one or a few shear bands. This leads to the brittle nature of metallic glasses. A way to improve the plasticity of shear bands is to increase the density of shear bands formed in the material.

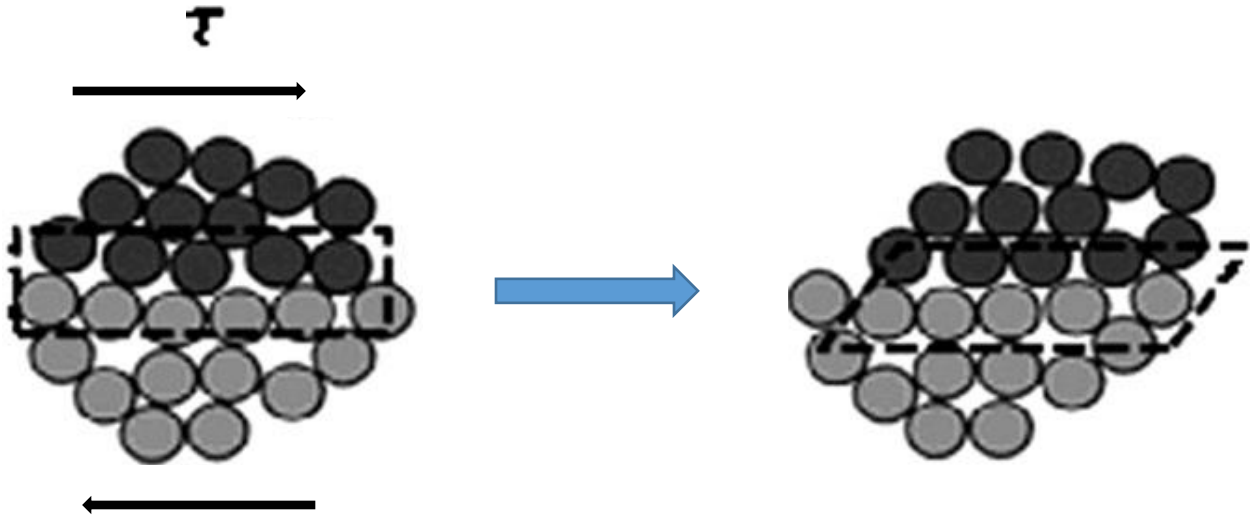

Figure 2.1: Schematic illustration of the STZ [4]

Spaepen [57] in 1975 was the first to propose the free volume theory that causes the deformation in metallic glasses. This theory suggested that the deformation is localized and viscosity change can arise due to this location resulting in the inhomogeneous plastic flow. While studying the failure surfaces of glassy alloys, typical vein patterns were observed confirming the low viscosity in the shear band. Moreover, the re-solidified droplet was observed on the fracture surface, which indicates localized melting or softening at the moment of fracturing [58]. The brittleness of metallic glasses is an overbearing disadvantage which limits their application as structural materials.

2.2.2 Strain Hardening in Amorphous Metals

Bulk metallic glasses are very popular for their remarkable strength and hardness. However, as stated earlier, BMGs generally possess very low tensile strain and no work hardening at room temperature. The mechanism of plastic deformation of glassy alloys is accomplished through the evolution of shear bands during applied shear stress and causes a localization of plastic flow [4],

[59], [60]. Due to this thermal softening effect, the bands form favorable sites for further plastic flow and as a result, leads to final failure caused by just one or very few shear bands [59], [60]. It has been widely observed that the way to improve the ductility and work hardening properties in BMGs is to suppress the localized strain softening caused by shear bands. Most reports on strain hardening in BMGs have been as a result of second phases being introduced into the amorphous matrix. In this way, the strain softening effect caused by the localized shear bands will be hindered by second phase particles introduced into the amorphous matrix.

By controlling the cooling rate and adjusting the alloy composition, a primary crystalline phase can precipitate preferentially. As cooling proceeds, the composition of the remaining melt deviates from the initial one and transforms into amorphous. Johnson and his team of researchers at Caltech, US [61] were the first to succeed at this method. They succeeded in synthesizing a Zr-based BMG composite with great plasticity and work hardening properties. They reported that this Zr-based BMG composite had excellent mechanical properties with a tensile ductility of 5 % and malleability of 6 %. The Bridgeman Solidification method was used by Qiao et al [62] [63] and Zhang et al [64] to synthesize their own BMG composites. These team of researchers both synthesized a Ti-based composite and observed excellent mechanical properties and ductility of 15.5 % at room temperature.

It is well known that amorphous alloys are not in thermodynamic equilibrium, therefore, a phase transformation process can take place when an adequate amount of external energy is supplied. Mechanical energy [54] and thermal energy [65] are two main driving forces that lead to this transformation. Mechanical energy, as a result of deformation, can lead to two main phenomena to occur.

Firstly, the deformation can lead to the formation of nanocrystallites near or along the shear bands. These nanocrystallites are known as deformation-induced nanocrystallites. Chen et al [54] bent an Al-based metallic glass and observed the surface of the bent sample using SEM and TEM. It was observed that nanocrystals were formed along the shear bands. Other researchers have also observed same phenomenon [66] [67].

The mechanisms involved in deformation-induced nanocrystallization is not clear yet but a number of suggestions have been proposed. Crystallization at elevated temperatures and deformation-induced temperature rise within the shear bands are evident phenomena in non-equilibrium metallic glass, it might be assumed that the nanocrystallization along the shear bands may be as a result of the high temperature caused by the dissipation of energy during shear deformation. However, in Wang et al's [67] study of a Ni-based MG with good glass forming ability, they concluded that the period of incubation of crystallization is about tens of seconds. Therefore, only the rise in temperature is not enough to cause nanocrystallization at such a short timescale. Other factors that could cause this in situ nanocrystallization may include high strain rates [68] and excess free volume produced during deformation [54].

Another phenomenon that could occur due to deformation is structural relaxation or densification. The mechanism is based on mechanically-driven relaxation of the glass structure. Wang et al. [69] showed that large hydrostatic tensile stresses led to diffusional relaxation of a Zr-based MG at ambient temperature. Packard et al. [70] also performed cyclic nanoindentation loading on a Fe-based metallic glass in the elastic range and observed considerable increase in hardness. They concluded that this increase in hardness was due to small structural changes including relaxation. The notion that deformation can lead to structural relaxation in metallic glasses has been widely reported [71]–[73].

2.2.3 Effect of Heat Treatment on Amorphous Materials

Heat treating a metallic glass below the temperature in which it crystallizes results in the transformation of its structure to a more relaxed state. This phenomenon is often called 'structural relaxation' and results in a change in all physical properties [74]. This structural relaxation can be observed with the aid of electron scattering or X-ray [75]. Quite a number of models have been developed to help explain the phenomenon of structural relaxation in metallic glasses. One of the models, which is the free volume model has been used extensively by researchers. This model is based on the surplus volume being confined to the material during quenching. The elimination and reshuffle of the free volume defects in metallic glass play a vital role in its properties.

Unique structural changes such as the decrease in free volume have been observed in metallic glasses after annealing below its glass transition or crystallization temperature. The metallic glass is metastable, which means that it can crystallize or exhibits structural relaxation when annealed at low temperatures. This structural relaxation can have an effect on the transport of atoms and other properties such as elastic, magnetic, electrochemical and so on. Annealing effects at relatively low temperatures should be minimal because of the low cooling rates of BMGs. Nonetheless, this annealing can alter the heat capacity and cause embrittlement of the BMG [76]–[79].

During the study of the microstructure of Vitreloy 105 [2], a Zr-based metallic glass, the alloy was annealed near its glass transition temperature. It was observed that small angle peaks were developed. This showed that there was a separation of phases in the supercooled liquid. Wang et al. also noticed the evolution of small angle peaks before crystallization during annealing experiments. This observation was also attributed to a separation of phases in the supercooled-liquid region taking place prior to crystallization [80]. Dmowski et al. [81], also observed structural

changes after annealing of their metallic glass. They performed hardness and DSC measurements and observed structural relaxation indirectly from those measurements. A relative increase in hardness was observed as annealing time and the temperature was increased. Furthermore, after annealing the metallic glass above its crystallization temperature, there was also a great increase in the Vickers hardness. The DSC scans also showed an evidence of structural relaxation. It was seen that the exothermic relaxation peak was accompanied by an increase near the glass transition temperature. So far, these researchers have shown an evidence of structural relation and increase in hardness due to annealing.

2.2.4 Size Effect in Metallic Glass

As stated in previous sections, the fundamental mechanism that governs the plastic deformation in glassy alloys is the shear bands. Because of this, explaining size dependence can be based on two possible perspectives. One could argue that properties of metallic glasses depend reasonably on their sizes because the size scale of mechanical testing is considerably above that associated with shear bands. Also, the idea that shear bands have a critical nucleus with diameter of about 50 to 500 nm [82] [83], proposes some size-dependence on the samples around that size.

Mg-based BMG with a diameter of about 12 μm was synthesized by Zheng et al in 2007 [84]. This BMG was synthesized using a dual Focused Ion Beam (FIB) and they observed a 3.2 % overall plastic strain. This micro-sized BMG showed size-dependent properties in comparison with the bigger samples of 1 and 4 mm which showed almost zero plasticity. That same year, the FIB method was also used to synthesize a Zr-based BMG by Guo and his team [85]. Reduction in the area at fracture of about 80 % was observed in their research. In addition to that, they observed great plastic strain of about 23-45 % and clear necking. Homogenous deformation was also observed by Jang and Greer [86] in their Zr-Ti-Co-Be metallic glass with ductility of about 6 %

before fracture. As regards tensile strain in metallic glasses, Wu et al. [87] displayed a fascinating study on size effect based on shear fracture and global ductility. They observed that tensile strain relies on the critical shear offset. As a matter of fact, the processes involved in the tensile fracture of BMGs are in three stages; first, the free volume begins to multiply and coalesce, this results in voids being formed and then a quick spread of shear crack.

The size-dependent tensile deformation of metallic glasses is understood in the sense that when the size of the specimen is decreased below the critical shear offset, there is a change in the shear deformation from unstable to stable, leading to a transformation from brittleness in relatively big sizes to large ductility in the microscale. On the other hand, Gu et al. [88] observed that the compressive plasticity of BMGs depends on the size of the sample. They attributed this size effects to the changes in Poisson's ratio for samples of the same composition fabricated in different sizes.

Many researchers have investigated the dependence of the strength of metallic glass on its size and also the way small samples deform during compression [89] [90] [91], and in tension [85]. While some of the researchers have recorded a dramatic change in strength due to size, some of them have observed no change [92] [93] [94].

2.3 Crystalline-Amorphous Composites

Metallic crystalline-amorphous composites are a promising new category of materials with unique physical and mechanical properties. In materials science, composites are materials that possess superior properties compared to the individual stand-alone materials. They comprise of reinforcements such as fibers, flakes and are embedded in a supporting matrix. Composite materials are designed for different purposes depending on their use. For instance, when a crystalline material is reinforced with metallic glass particles, the main goal is to improve strength.

On the other hand, when metallic glass is reinforced with crystalline particles, both strength and ductility can be improved. Three different ways of synthesizing crystalline-amorphous composites are discussed in this section.

2.3.1 Synthesis of Crystalline-Amorphous Composites

The synthesis of these composites can be divided into three main methods depending on their phases. These methods are Melting and Quenching (Liquid), Sputtering (Vapour) and Accumulative Roll Bonding (Solid)

2.3.1.1 Melting and Quenching

This method involves melting the master alloy and then rapidly cooling the ingot at very high cooling rates of about 10^5 K/s or more. To achieve this kind of cooling rate, the ingots are made to come in contact with a surface that possesses high thermal conductivity at a high speed. The melt spinning technique for melting and quenching has been used by researchers to synthesize both pure metallic glass [95]–[98] and C-A composites [6], [99]–[102]. It involves driving the material from a nozzle in form of a jet, to a rotating disc/roller. Because of the temperature difference between the molten alloy and the rotating disc, the melt solidifies into a ribbon.

Despite the breakthroughs achieved in this method of synthesizing C-A composites, there have still been some limitations. These limitations include the need to safely handle the rapid solidification products, some of the dimensions achieved during the melt spinning process restricts the use of the products for design and construction and also prevents a detailed investigation into its mechanical properties [103]. Also, the formation of crystalline phase is very sensitive to cooling rates [104]. A slight change in the cooling rates can cause a massive variation in the microstructural configuration.

2.3.1.2 Sputtering

Deposition of materials unto a substrate has been used commercially for many years. One of these types of decomposition is called Sputtering. It is a physical vapour deposition (PVD) process which involves discharging atoms from a material and compacting the discharged atoms in a high vacuum system onto a substrate. The process of sputtering is as follows; energetic ions such as Argon are bombarded on the material that is to be deposited. Target atoms are now ejected into space due to the forceful collision of these ions. Some distance is then traveled by the ejected atoms until they arrive at the substrate and start to compact into the film. Bonding between the atoms now begins at a molecular level as more atoms arrive at the substrate, forming a tightly bound layer of atoms. Depending on the time required for the sputtering, more than one layer can be created. This process has been used to synthesize crystalline-amorphous composites [7] [105] [106], where amorphous particles on being deposited on crystalline materials and vice versa.

As easy as sputtering may seem, the actual technique is quite complex. Furthermore, preparation of bulk crystalline-amorphous composites is still very challenging.

2.3.1.3 Accumulative Roll Bonding (ARB) Process

Saito et al were the pioneers of the ARB process in 1998 [107]. ARB is a severe plastic deformation process used by researchers to synthesize ultrafine grained metallic materials. The ARB process involves stacking materials together and rolling them into one body of material. Because of this, ARB is a deformation process as well as a bonding process. The rolled material is then cut in half, stacked and rolled again, hence, “accumulative roll bonding”. To ensure effective bonding between the materials, the material’s surface is usually degreased and roughened before stacking. On some occasions, warm rolling is carried out. This involves heating the stacked materials to an elevated temperature, usually below the temperature of recrystallization and then rolling. Furthermore, to

achieve effective bonding, the reduction in thickness before and after rolling should be at least 50 %. Figure 2.22 shows the overall process of ARB. This procedure can be repeated as many times as possible, so that very substantial amount of strain is applied to the material.

After *n* number of cycles, the strain applied to the material can be expressed as;

$$\varepsilon = \frac{\sqrt{3}}{2}\ln(r) \qquad \text{Equation 2-3}$$

$$r = 1 - \frac{t}{t_0} = 1 - \frac{1}{2^n} \qquad \text{Equation 2-4}$$

Where t_0 is the starting thickness of the stacked sheets, *t* is the thickness after the roll-bonding and r is the thickness reduction per cycle.

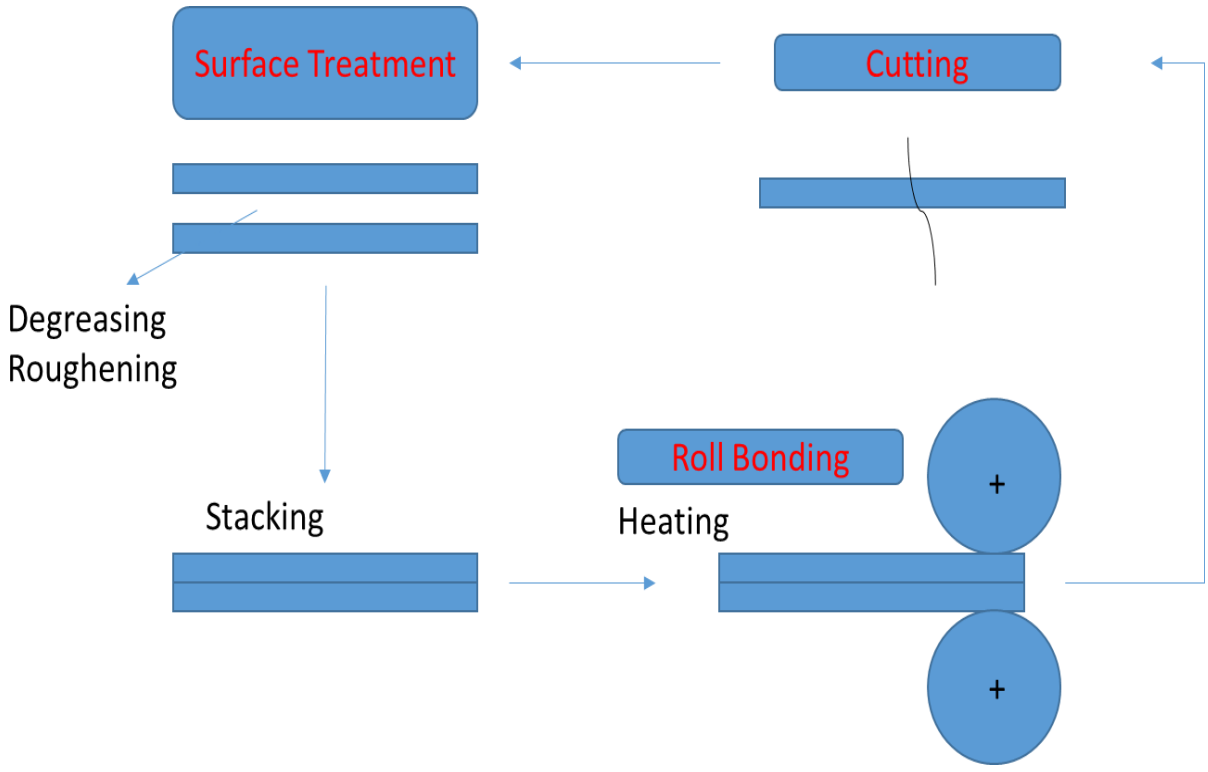

Figure 2.2: Simplified Illustration showing the principles of ARB

The deformation and bonding mechanisms of the materials during ARB can be explained based on plastic instability, caused by the difference in properties between each phase. When two materials with a substantial difference in hardness are rolled, necking and subsequent fracture of the harder phase is observed [108]–[111]. Necking is a phenomenon in which a local region of a material experiences decrease in cross-sectional area due to a large amount of tensile strain. Due to necking, the hard phase starts to fracture and is distributed as particulates in the soft phase. The soft phase can then flow and penetrate into each other, leading to bonding.

As earlier stated, the ARB process was invented by researchers to fabricate ultrafine grains. More recently, this process has also been used to synthesize C-A composites [8], [112]. Researchers have recorded a Solid State Amorphization Reaction (SSAR) while bonding two or more crystalline materials. The mechanisms for this SSAR involves two modes which are the mechanically activated and thermally activated modes. These modes are due to strain caused by the rolling process as well as annealing.

Unlike the amorphization reaction described above, my research is focussed on bonding an already synthesized metallic glass with a crystalline material to achieve a C-A composite. The ARB process is used because it is relatively cheap compared to the other methods described above. Also, the ARB process enables us to fabricate a long role of material without a significant restriction in the size of the synthesized sample. Therefore, this method is advantageous is fabrication bulk C-A composites.

2.3.2 Properties of Crystalline-Amorphous Composites

Crystalline-Amorphous composites would possess a good amount of strength and plasticity due to the interaction between shear bands and the crystalline material at the interface between the

crystalline and amorphous material. The main idea is to increase the amount of shear band formation, so as to dissipate the energy of deformation into a larger volume and to get rid of stress concentration, in order to improve plasticity.

In 1997, Kato and Inoue [113] incorporated ZrC particles into $Zr_{55}Al_{10}Ni_5Cu_{30}$ BMG and they observed a significant increase in strength and plasticity. Fu et al. [114] introduced TiB into $Cu_{47}Ti_{33}Zr_{11}Ni_6Sn_2Si_1$ BMG, with different volume fractions TiB. Johnson and his team of researchers [115] [116] reinforced $Cu_{47}Ti_{34}Zr_{11}Ni_8$, $Zr_{52.5}Ti_5Al_{10}Cu_{17.6}Ni_{14.6}$ and, $Zr_{52.5}Ti_5Al_{10}Cu_{17.6}Ni_{14.6}$ with SiC and WC particles and observed a plasticity of around 3 to 7 % under compressive test.

Asides ceramic materials, the BMGs can also be reinforced with other particles. Choi-Yim et al [116] [117] incorporated W, Ta, Mo, Nb into V106, and subjected the composite to compressive loading. They observed a dramatic improvement in plasticity as a result of the evolution of several shear bands formed as a result of the reinforcing particulates. Mg-based BMGs have also been reinforced with other metal particulates such as Fe [118], Nb [119], and porous Mo [120]. These particulates have increased the plasticity of the BMG to between 10 to 40 %.

This method of reinforcement for BMGs can be divided into two categories; one of which is the “hard’ phase reinforced BMG composite and the other is the “soft” phase reinforced BMG composite. In the latter case, when the loading is compressive, the soft phase will deform first, and there will be an accumulation of stresses at the interface between the matrix and the soft phase. At a point in time when the stress concentration reaches a crucial value, the first shear band will be generated. The shear band formation will decrease the stress around the particle. Since the particles are distributed around the matrix, the shear band will also form in other regions where the stress concentration reaches a critical value. In this way, multiple shear bands will develop and move

throughout the composite material. The shear band will propagate to the direction of neighbouring particles. This will make it impossible for the shear bands to propagate without being blocked or pinned or absorbed. When these shear bands are blocked, other shear bands begin to form and so on. This will lead to a homogeneous distribution of shear bands and strengthening of plasticity [61], [121].

As for the former case, the matrix will deform first and the shear bands will be initiated within the matrix material. Similar to the case of the "soft" phase, there will be stress concentration at the interface between these two different phases, leading to the emergence of multiple shear bands. When propagating shear bands reach the harder second phase, they will deflect or change direction. In both of these cases mention, the effect of the interaction between the softer and harder phases lead to the formation of multiple shear bands. For shear bands to get through the harder phases, a higher force is required to be applied. Therefore, BMGs that are strengthened with the hard phase have superior strength [122]–[124] and less plasticity compared with the ones reinforced with the soft phase.

2.4 Nanoindentation

Nanoindentation is a non-destructive technique that is used to evaluate the local mechanical properties of materials. It can measure properties of materials even when they are only available in small sizes. Due to this, the technique has gained the attention of many researchers. Nanoindentation is quite unique and different from conventional hardness tests. Load-displacement curves are plotted while the loading and unloading sequence is going on and mechanical properties are measured from these curves. In the recent past, chemists, organic and inorganic materials have been tested by nanoindentation to evaluate their mechanical properties

[125]–[129]. Engineering researchers have also used this method to evaluate the mechanical properties of poly-crystals, single crystals and amorphous materials [130]–[135]

2.4.1 Principles of Nanoindentation

The main goal of nanoindentation is to estimate the Hardness, H and Young's Modulus, E of a material. This is accomplished by analyzing the load-displacement curves after indentation. Figure 2.3 represents a cross-section of a typical nanoindentation and shows the parameters used in the analyzing the results. A typical example of a load-displacement curve is shown in Figure 2.4.

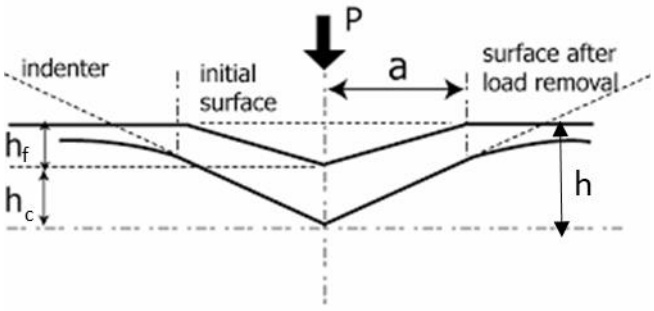

Figure 2.3: A simple representation of how the indentation works showing various quantities used in the analysis [136]

The nanoindenter is a very sensitive instrument, therefore there is need to carefully select the parameters for testing involved in the indentation. These testing parameters include the maximum load (P_{max}) or the maximum displacement (h_{max}), and the rate at which the indentation is performed. Nanoindentation experiments are similar to the uniaxial tensile test in the sense that they can be utilized either in load-controlled or displacement controlled modes. While the load-controlled mode involves prescribing the loading and unloading rates (dP/dt) and P_{max}, the displacement-controlled mode, involves keeping (dh/dt) and h_{max} constant and the indention rate is set as the displacement rate.

The most widely used technique for evaluating the material's hardness and modulus is the method presented by Oliver and Pharr [136] in which H, which is equivalent to the mean contact pressure, P_m is defined as;

$$H = \frac{P_{max}}{A_c} \qquad \text{Equation 2-5}$$

Where A_c is the proposed contact area. A_c is a numerical function of the contact depth, h_c. Considering an idealized Berkovich tip, $A_c = 24.5h_c^2$. Because the tips get more and blunter during their usage, these tips have to be recalibrated occasionally to determine the practical relationship between A_c and h_c. Oliver and Pharr [136] also suggested that the contact depth is given by:

$$h_c = h_{\max - \omega} \frac{P_{max}}{S} \qquad \text{Equation 2-6}$$

Where ω is a geometric parameter; for a cone probe, $\omega = 0.72$, 0.75 for a rounded tip, and 1 for a flat punch. For the Berkovich tip, $\omega = 0.75$, which is a three-sided pyramid.

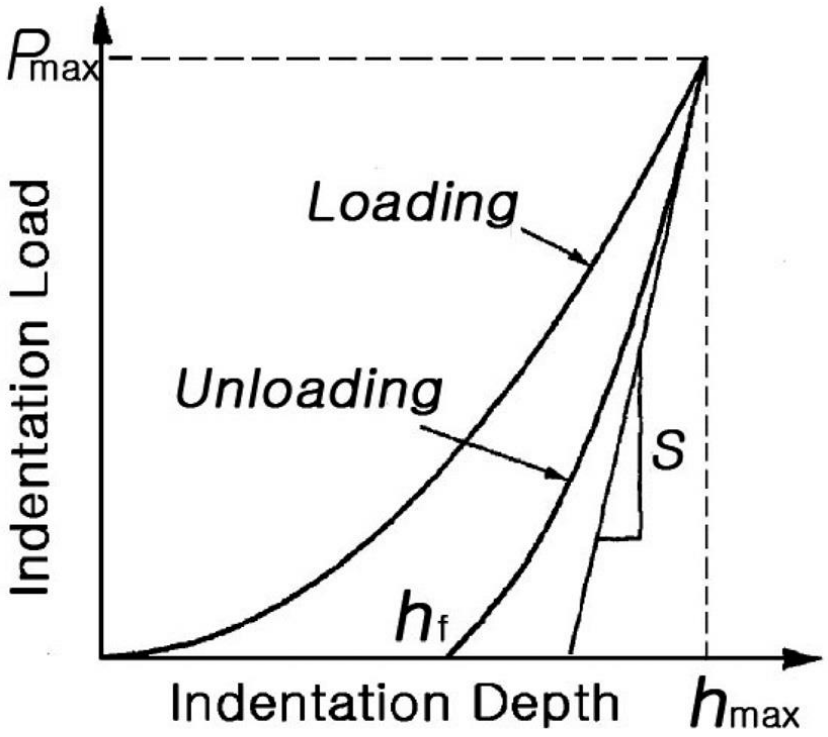

Figure 2.4: Typical representation of a load-displacement curve after the loading and unloading sequence [136]

S, which is the stiffness while unloading is the initial gradient of the loading curve (see figure 2.4) and is evaluated as follows; the power law relation, $P = B(h - h_f)^m$ is used to fit the unloading curve, where B and m are fitting parameters and h_f is the final displacement after the unloading sequence has been completed. After that, S is then evaluated by differentiating this relation and setting $h = h_{max}$ such that $S = dP/dh|_{h = hmax}$.

When S and A_c have been evaluated, it is then possible to determine the reduced modulus, E_r, of the indented material through the elastic contact theory [136] [137].

$$E_r = \frac{1}{\beta}\frac{\sqrt{\pi}}{2}\frac{S}{\sqrt{A_c}} \qquad \text{Equation 2-7}$$

Where β is a constant that depends on the indenter geometry. The value of β for the Berkovich indenter is 1.034.

2.4.2 Nanoindentation in Crystalline and Amorphous Metallic Materials

Nanoindentation has been used to evaluate the mechanical properties of crystalline and amorphous materials by various researchers [32], [138], [147], [139]–[146]. While the load-displacement plots of most crystalline metals show smooth curves (as in Figure 2.4), that of the amorphous metallic glass exhibits a discontinuity in the load-displacement curves.

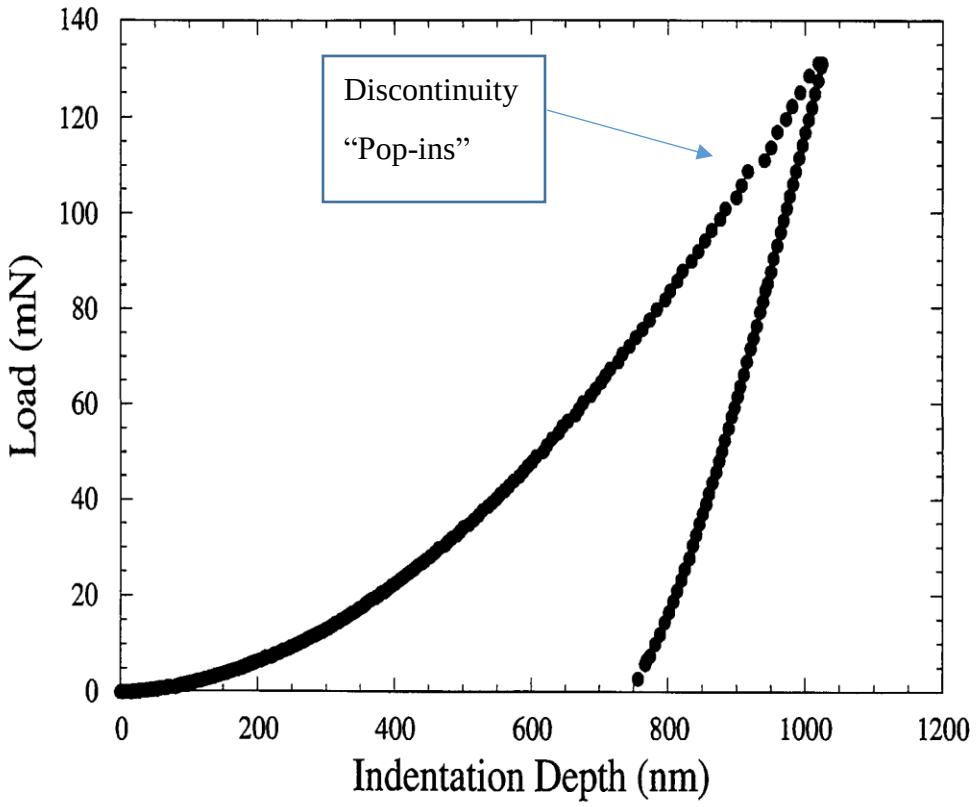

Figure 2.5: Typical Example of Load-Displacement Curves Showing Pop-ins [143]

Wright et al [143] observed these discontinuities and attributed this “pop in” event to the formation of shear bands under the probe tip. These “pop-ins” are the only proof of shear band activity on the load-displacement curves.

Chapter 3 - Methodology

This chapter is assigned to explain the details of the methods involved in the current study. The experimental details include material selection, synthesis of the composite using ARB, material characterization and nanoindentation. These methods will be discussed in detail in this chapter.

3.1 Sample Preparation

3.1.1 Material Selection

Crystalline copper sheets were purchased from ThyssenKrupp Materials NA supplier. Based on the data sheet provided by ThyssenKrupp Materials NA supplier, the copper sheets were ~99.9 % pure. The Nickel sheets were purchased from onlinemetals. From the data provided, the nickel sheets were 99% pure. A roll of metallic glass, on the other hand, was purchased from Goodfellow limited. The metallic glass is an alloy of nickel, silicon, and boron. The details of the compositions of both copper and metallic glass are given in table 3.1 and table 3.2 respectively. The thickness of the as-received copper was 508 µm while that of the as-received metallic glass was 25 µm. All samples used for this study were prepared from the sheets described above.

Table 3.1: Composition of as-received Cu material based on supplier's data sheet

Cu sheet	Cu (%)	Ag	S	Fe	Pb	Ni	O
(ppm)	99.99	25	15	10	5	10	5

Table 3.2: Composition of as-received Ni material based on supplier’s data sheet

Ni sheet	Ni	C	Cu	Fe	Mn	S	Si
%composition	99	0.15	0.25	0.4	0.35	0.01	0.35

Table 3.3: Composition of as-received metallic glass based on supplier's data sheet

Metallic Glass	Ni	Si	B
% composition	78	8	14

The crystalline copper and nickel were selected because they are commercially available and cheap. Copper also be used and has been proven effective for ARB processes [139], [148]–[150]. The nickel-based metallic glass is also commercially available and easy to fabricate. This metallic glass was also suitable for ARB processing by the rolling machine housed in the materials processing laboratory at the University of Manitoba.

3.1.2 Accumulative Roll Bonding (ARB)

A 50 Ton STANAT rolling machine was used for the ARB operation. The procedures followed for the ARB process are given in detail below;

1. The Cu sheet and metallic glass strip were cut into samples of length 5 cm and width of 5 cm.
2. The samples were then dipped in acetone for 5 minutes for cleaning and degreasing.
3. The surface of the copper strip was scratched using a steel wire brush and the metallic glass surface was scratched using a sandpaper. The sandpaper was used instead of the steel wire brush because the metallic glass was too hard for the wire brush to scratch.
4. After brushing, a sandwich of 7 layers, four layers of copper and three layers of metallic glass, was prepared so that the harder metallic glass sample will be between the soft copper samples. Figure 3.1 shows the schematic of the sandwich made as well as the corresponding thicknesses.

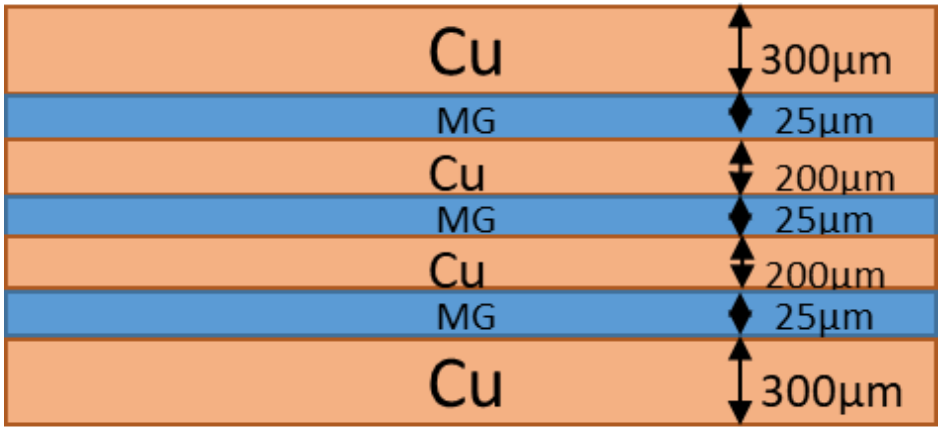

Figure 3.1: Schematic of the sandwich prepared for the ARB process

5. Holes were created on the samples and the layers were fastened using wire strips as shown in figure 3.2 below. This was done to prevent sliding during the ARB process. These wire strips were removed after each ARB process.

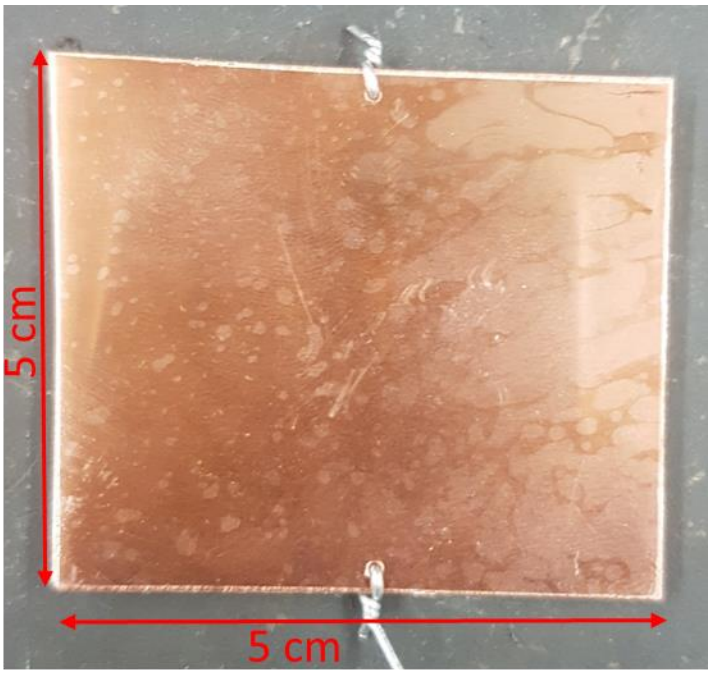

Figure 3.2: Cu-MG-Cu sample fastened using wire strips

6. After the sandwich preparation, the gap between the rollers of the machine was adjusted and then the sample was rolled. The gap was adjusted so as to obtain at least 50 % reduction in thickness. It should be noted that when the reduction is above 70 %, the sample starts to bend and bonding becomes less effective.
7. After rolling, the edge of the samples was cut to remove the wire strips and edge cracks that formed during the rolling process.
8. The sample was then cut in half and the procedure was carried out from step 2 to step 7 all over again. Figure 3 below shows the schematic representation of the whole ARB process.

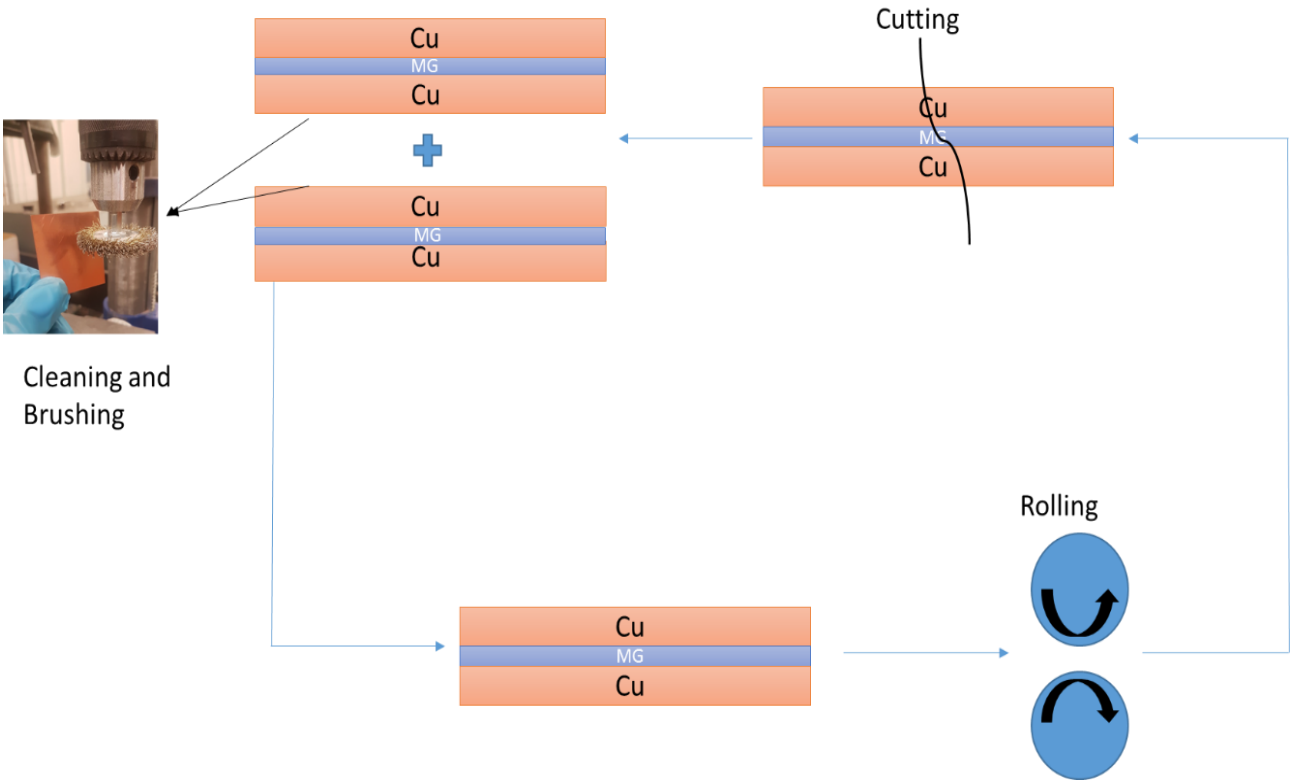

Figure 3.3: Schematic view of the ARB process

9. A piece was cut from the sample after each rolling pass for material characterization and nanoindentation.

The same process was utilized for the nickel and metallic glass sheets. Only one ARB cycle was performed on the nickel and metallic glass sandwich followed by heat treatment.

3.2 Material Characterisation

X-ray diffraction technique was used to determine the structure of the metallic glass. In order to examine the microstructural evolution of the synthesized samples, two main microscopy techniques were used. The optical microscopy (OM) and the scanning electron microscopy (SEM). Also, DSC technique was used to investigate the thermal properties of the samples.

3.2.1 X-ray Diffraction

XRD was carried out on the as-received metallic glass using a Siemens D5000 diffractometer. A small sample of the metallic glass was cut and mounted on a stage in the X-ray chamber. The instrument uses a Bragg-Brentano geometry to carry out the test. The MG was bombarded with Cu X-rays. The data collection parameters were as follows;

Scan 2θ: $20^o - 60^o$

Step Size: 0.02^o

Step Time: 1s

3.2.2 Optical Microscopy

The cross-section of each of the samples was mounted and polished to reveal their microstructure and to study the microstructural evolution of the Cu/MG system and the Ni/MG system after each rolling pass. The mechanical polishing of the mounted sample was done using a rough 600 sandpaper and then it was gradually changed to a finer 1200 sandpaper and then to smoother 6 and 1-micron clothes. During the polishing, water and diamond suspension fluids were used as lubricants. The samples were then washed and cleaned for microstructural examination. The microstructure of the samples was examined by optical microscopy using an inverted-reflected light microscope with CLEMEX Captiva vision 3.0 image processing software.

3.2.3 Scanning Electron Microscopy

The interface between the crystalline copper and amorphous metallic glass was observed using the JEOL 5900 scanning electron microscope. The secondary and back-scattered electron detectors were used in imaging the cross-section of the samples. This procedure was also preceded by sample preparation which involved mounting and polishing the sample.

3.2.4 Differential Scanning Calorimetry

The crystallization temperature of the as-received metallic glass and the metallic glass in the copper matrix were investigated using a TAM Air DSC under high purity dry nitrogen. Ceramic pans were used as sample holders. The heating rate for the test was set at 10 ^{o}C/min and the cooling was done at room temperature.

3.3 Nanoindentation

The hardness and elastic modulus of all samples were measured using the Hysitron TI Ubi Nanoindenter. The Berkovich tip, which is the most widely used probe in nanoindentation was used for the test. Nanoindentation was performed at room temperature and all tests were conducted based on a standard load function shown in figure 3.4 below.

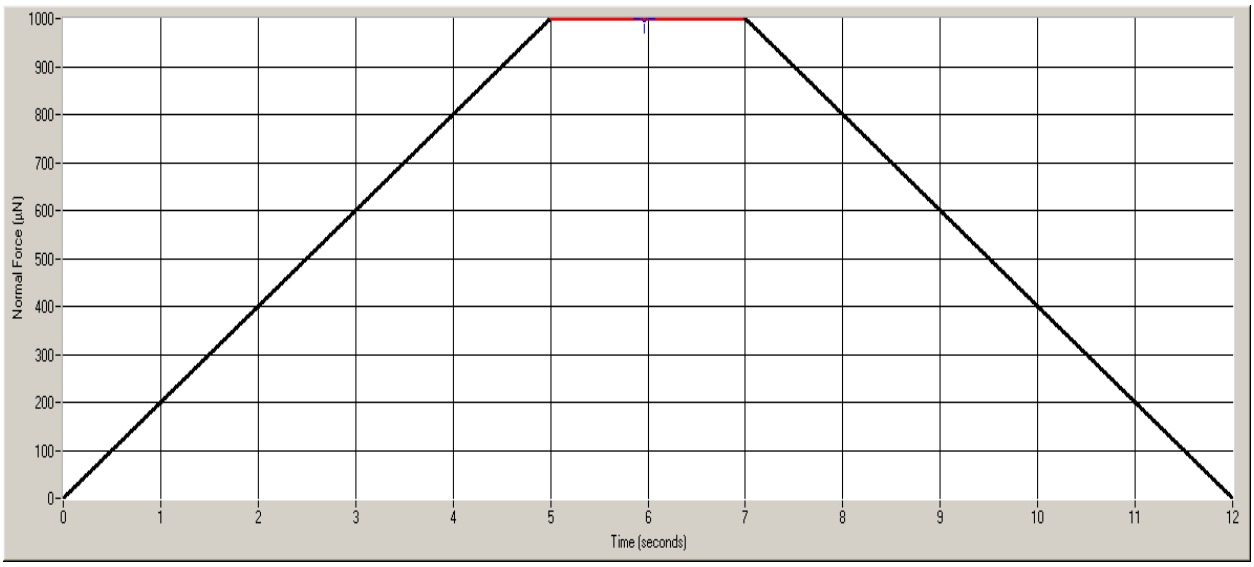

Figure 3.4: Standard Trapezoid Load Function Used in Nanoindentation

The load-controlled mode was used for the testing and the maximum force was set at 5000 μN. The spacing between indents was 2 μm to avoid shear band interaction between two adjacent indents. All results were extracted using the Hysitron software.

Chapter 4 - Results and Discussion

This chapter presents the results and discussion of the experiments and analysis described in chapter 3. Sections 4.1 – 4.4 are based entirely on the experiments and analysis performed on the Cu/MG system. Section 4.5 presents a comparison between the Ni/MG system and the Cu/MG system.

4.1 XRD on Pure Metallic Glass

The XRD results for the as-received metallic glass sheet used for this research is shown in Figure 4.1. As can be seen, the sheet exhibits an almost fully amorphous structure confirmed by a presence of a broad diffraction peak around 45^0.

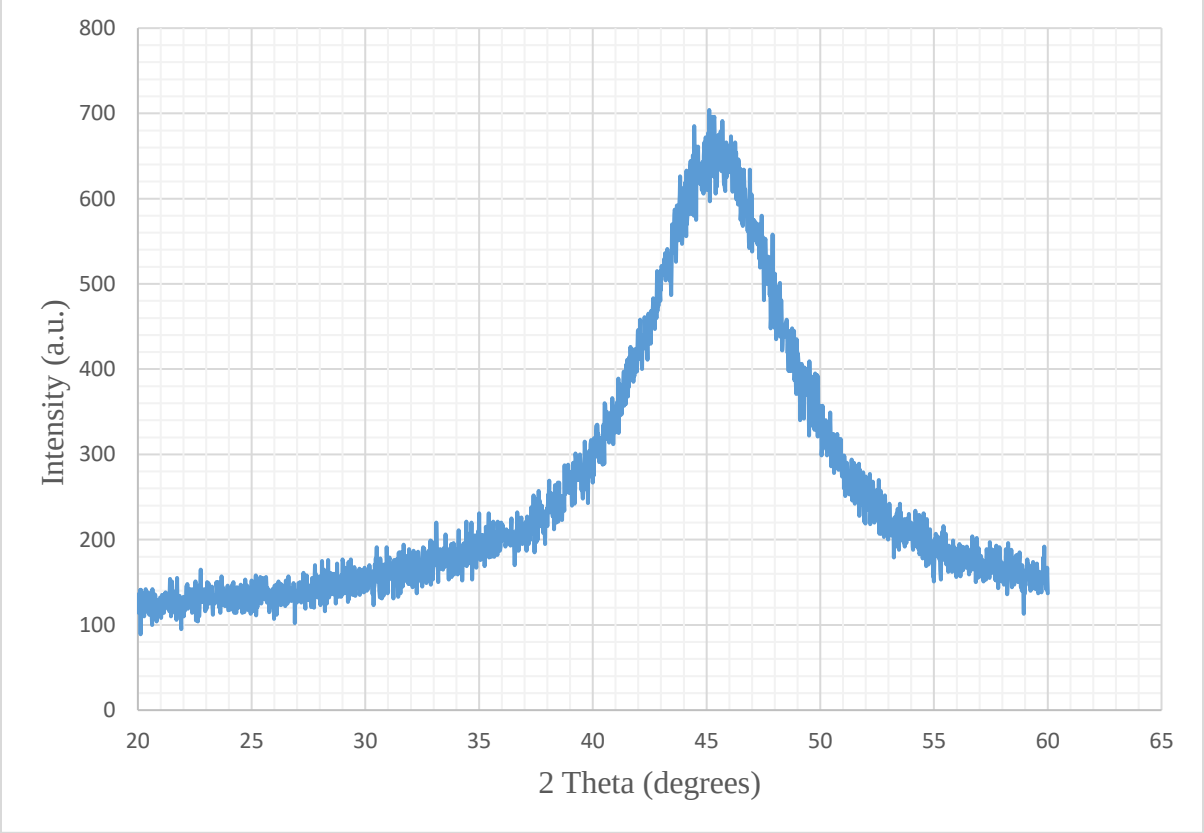

Figure 4.1: X-ray diffraction of the Ni-based metallic glass

4.2 Microstructural Analysis

The microstructural analysis of the samples made following the procedure in chapter 3 was done in two steps. First, the optical microscope was used to observe the microstructural evolution of the Cu/MG system as the number of passes increased. The microstructural evolution of the Cu/MG and Ni/MG systems are similar, hence the Cu/MG system is presented in this section. In addition to that, the SEM was used to examine the bonding between the crystalline copper and amorphous structure at the interface.

4.2.1 Microstructural Evolution during ARB

Figure 4.2(a) illustrates the optical micrograph of the Cu/MG system after the first ARB cycle. It can be observed that the metallic glass fractured just after one pass. This is because of the very brittle nature of the glass as explained in section 2.2.1. In general, it has been reported that necking and subsequent fracture takes place in the harder phase as a result of simultaneous deformation of dissimilar metals and the difference in flow properties of the constituent phases [151] [152]. The plastic instability is governed by the initial thickness ratio of the layers, strength coefficients, and strain hardening exponents [153]. In the case of the Cu/MG system, the metallic glass acts as the hard phase and fractures.

Figures 4.2(b), 4.2(c) and 4.2(d) shows the optical micrographs of the Cu/MG system after the second, third and fourth ARB cycles respectively. Following the ARB cycles, it was observed that as the number of cycles increased, the metallic glass broke into smaller fragments and was distributed in the copper matrix. It should be noted that during ARB of bimetallic systems where the initial thickness of the hard phase is smaller than that of the soft phase, the final microstructure is composed of fragmented hard phases being uniformly distributed within the soft matrix [108], [110], [111], [154].

(a) step 1

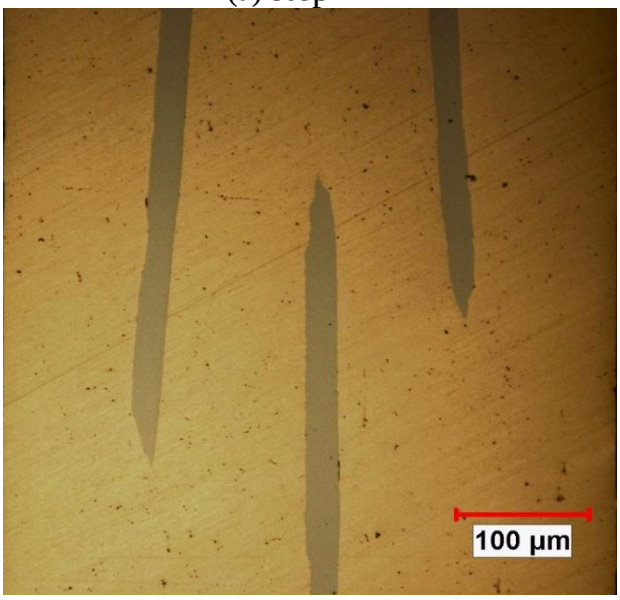

(b) step 2

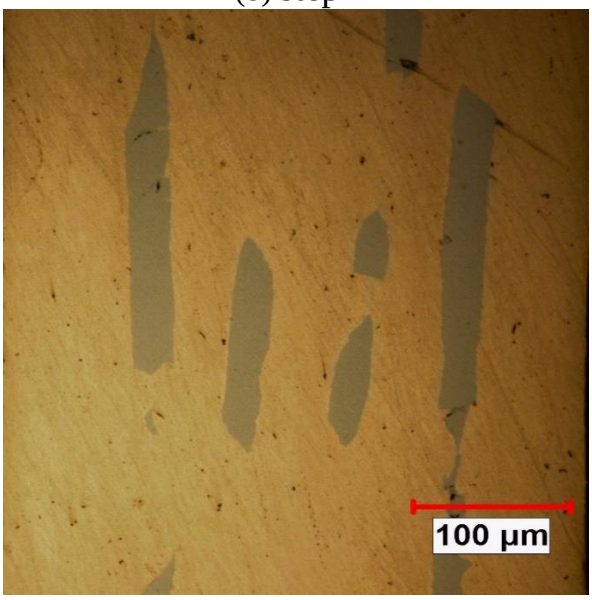

(c) step 3

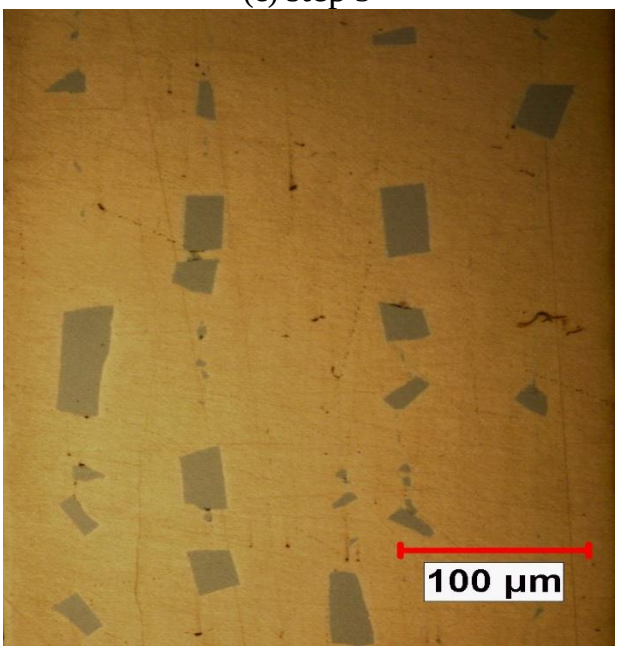

(d) step 4

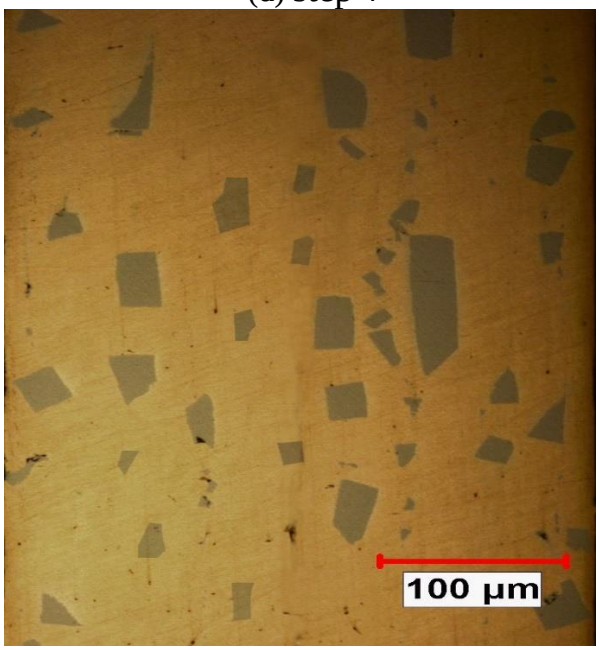

Figure 4.2: Optical micrograph of the Cu/MG system after (a) 1st, (b) 2nd, (c) 3rd, and (d) 4th cycles of rolling.

4.2.2 Bonding of the Cu/MG System

One of the main characteristics of the ARB process is that it is not just a rolling process but it is also a bonding process. Bonding is essential during the process to ensure continuity along and across the cross-section. Figure 4.3 shows an SEM image of the microstructure variation of crystalline copper and amorphous metallic glass. No apparent voids or discontinuities were seen at the straight bonding boundary of the Cu/MG system, indicating that the layers were well bonded together even after the first cycle. The Cu-Cu boundary could not be seen as well, clearly indicating that the two layers were also effectively bonded together.

Figure 4.4 shows an EDS line-scanning analysis across the Cu-MG-Cu laminated composite after the fourth cycle. As shown in the figure, no significant inter-diffusion was observed.

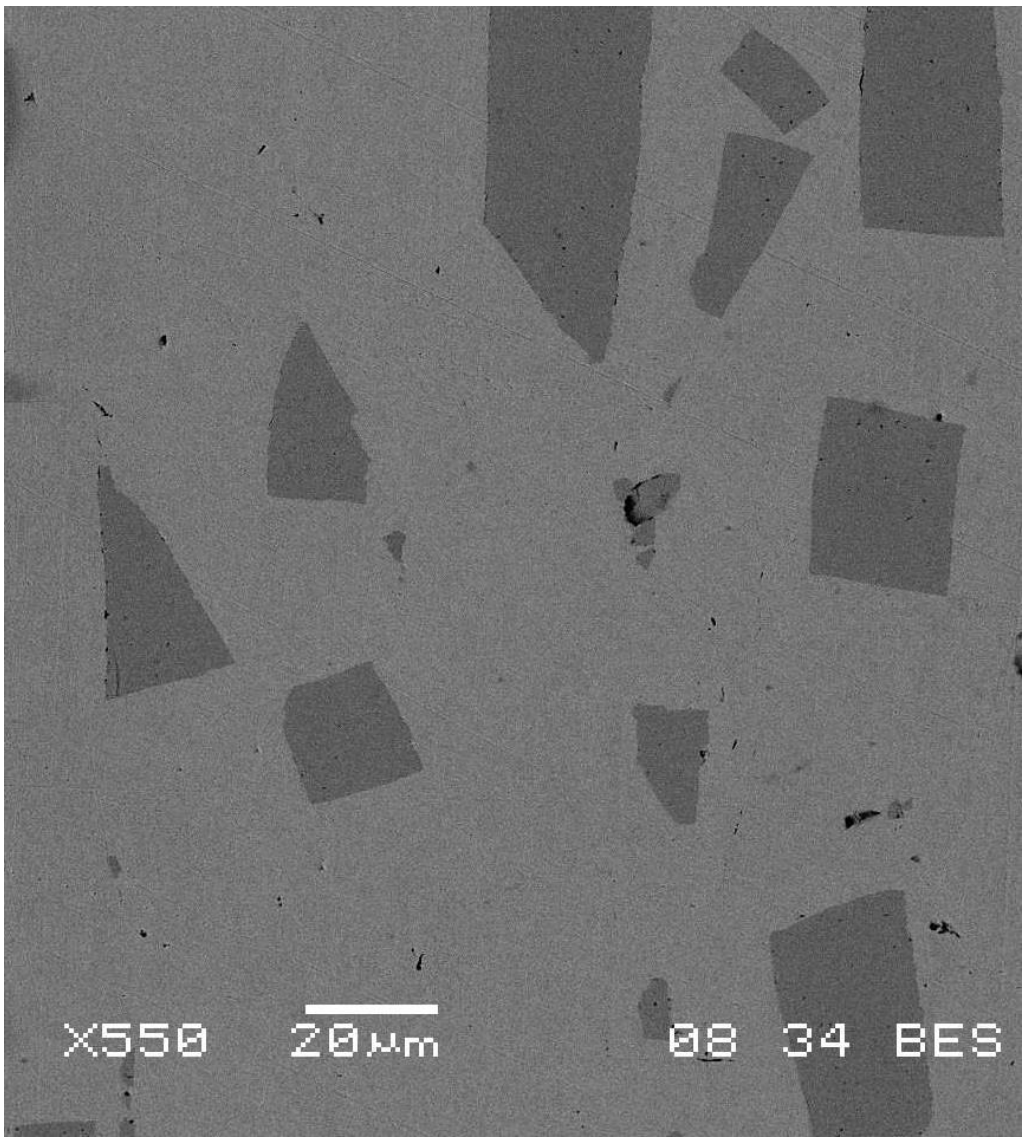

Figure 4.3: SEM image of the Cu/MG system after the fourth pass showing the Cu-Cu and Cu-MG laminated layers

Figure 4.4: EDS line scan across Cu, MG and Cu layers

4.3 Nanoindentation

The properties of a bulk composite are greatly affected by the properties of the reinforcing materials. Due to the processes involved during ARB, this research involves determining the properties of the reinforcing material as a result of those processes. As earlier mentioned, nanoindentation experiments were conducted on the metallic glass region of the composite mainly because the sizes of the metallic glass fragments are in submicron level. Hence, the use of this sophisticated instrument to characterize the properties of the metallic glass. Hardness and elastic modulus are the two main properties that can be extracted from nanoindentation. The hardness and

elastic modulus due to strain, heat treatment, and size of the metallic glass is explained in this section. Strain imposed and heat treatment is two major processes involved during ARB. Three different samples were prepared and used for the nanoindentation testing for precision and accuracy.

4.3.1 Hardness

Hardness is a material ability to resist localized plastic deformation usually either by indentation or penetration. The hardness property of the reinforcing material is described in this subsection due to strain, heat treatment, and size.

4.3.1.1 Effect of Strain on the Hardness of Metallic Glass

As the number of ARB cycles increases, so does the strain imposed on the Cu/MG system. Unlike the crystalline copper that exhibits strain hardening, work hardening is rarely observed in metallic glass. Figure 4.5 shows a plot of the hardness of the metallic glass against the number of ARB cycles. It is important to note that intermediate heat treatment was not performed during the bonding process. It can be observed that the hardness of the metallic glass increased after the first cycle and continued to increase with increasing number of cycles. According to Stolpe et al [155] who performed cold rolling on the metallic glass, the density of shear bands increased as the amount cold rolling was increased. They also concluded that the density of shear bands formed was based mainly on the plastic strain applied and not due to the chemical composition of the metallic glass.

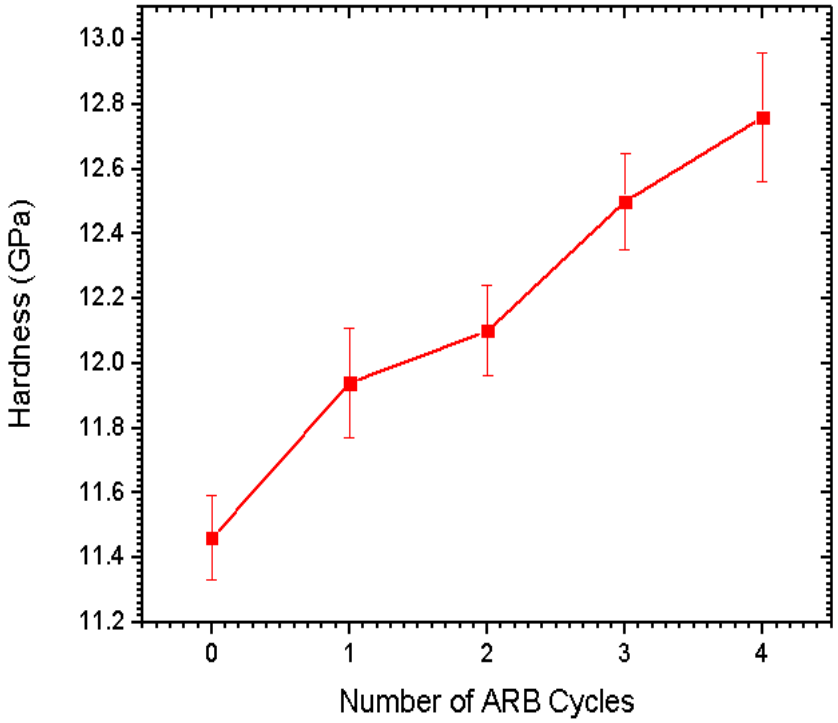

Figure 4.5: Graph of the hardness of the MG against number of ARB cycles

During the ARB process, compressive stress was induced on the metallic glass which led to the formation of shear bands. As discussed in section 2.2.2, the formation of shear bands likely led to deformation induced nanocrystallization. Therefore, during nanoindentation, these nanocrystallites possibly impeded the propagation of shear bands leading to a lower deformation area. Since hardness is a function of applied force and area as discussed in section 2.4.1, this process would have led to an increase in the hardness of the metallic glass. Also, the compressive stresses induced may have led to structural relaxation. As a result of this structural relaxation, atoms are more closely packed, atomic bonding energy increases, and free volume is reduced, resulting in the increase in the hardness of the metallic glass during nanoindentation. One or both of these phenomena could have led to the overall increase in the hardness of the metallic glass.

4.3.1.2 Effect of Heat Treatment on the Hardness of Metallic Glass

One of the ways to improve bonding during the ARB process is to anneal the base material after each ARB cycle to recover some ductility. This is why the effect of this heat treatment was studied for the metallic glass. The Cu/MG system after one ARB cycle was annealed using a Carbolite Gero furnace. The annealing was done at temperatures below the crystallization temperature of the metallic glass. Before this annealing was performed, a DSC analysis was done to determine the crystallization temperature of the metallic glass. Figure 4.6 shows the DSC plots. As it can be observed from the peak in the DSC curve, the crystallization temperature of the metallic glass was found to be around 505 ^{o}C. Annealing was performed on the Cu/MG system at temperatures of 100^{0}C, 200 ^{o}C, 300 ^{o}C and 400 ^{o}C.

Figure 4.7 illustrates a plot of the hardness of the metallic glass as a function of temperature. It was observed that that at low temperatures of 100^{o}C and 200 ^{o}C, there was no effect on the hardness of the metallic glass. But as the temperature increased above 200 ^{o}C, so did the hardness of the metallic glass.

On higher temperature annealing of above 200 ^{o}C, structural relaxation likely occurred in the metallic glass. This led to a reduction in free volume which might have also led to short-range ordering. This structural relaxation results in impeding the movement of shear bands or an increased resistance for the nucleation of shear bands in the material which in-turn leads to an increase in the hardness value of the metallic glass. Structural relaxation and annihilation of free volume have been reported in earlier studies [156] [157]. There is an obvious energy barrier for structural relaxation to begin to occur. This may be the reason why hardness values did not change at lower temperatures.

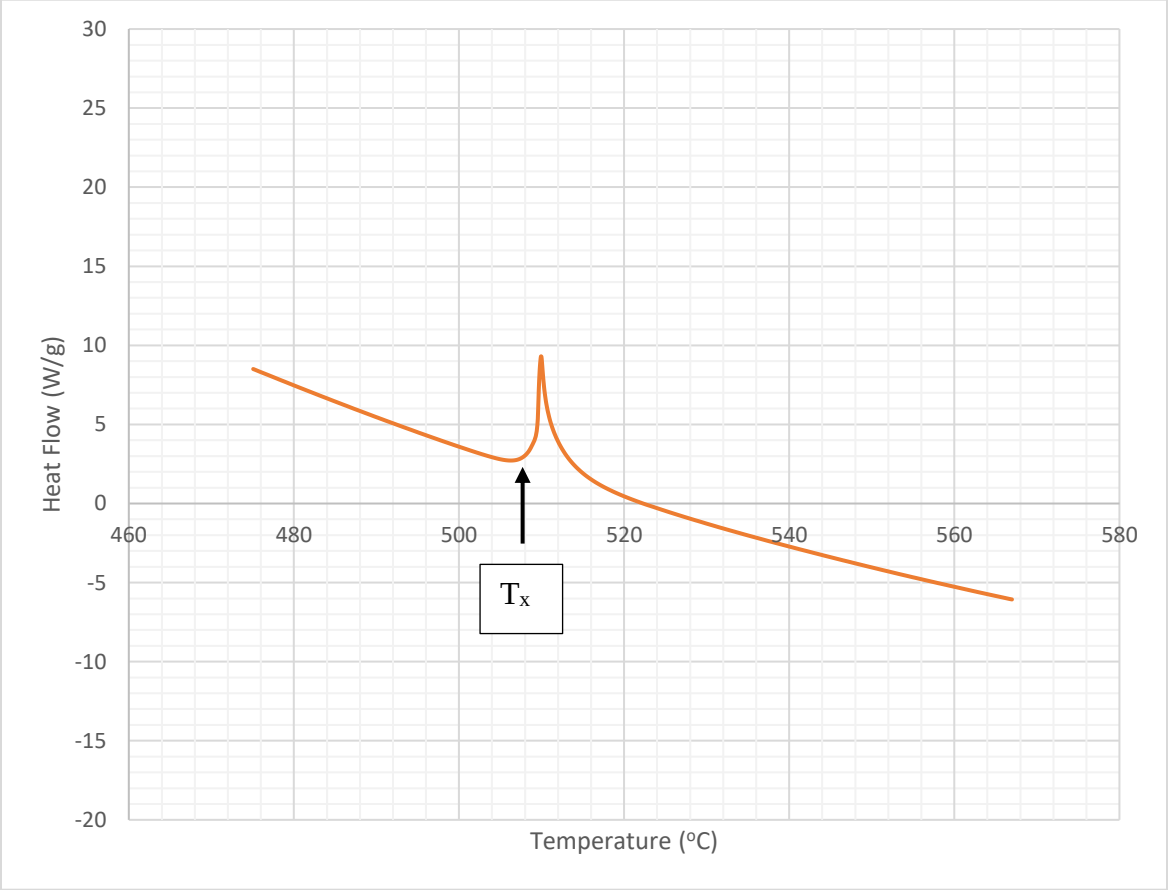

Figure 4.6: DSC plot indicating the crystallization temperature of the as-received metallic glass

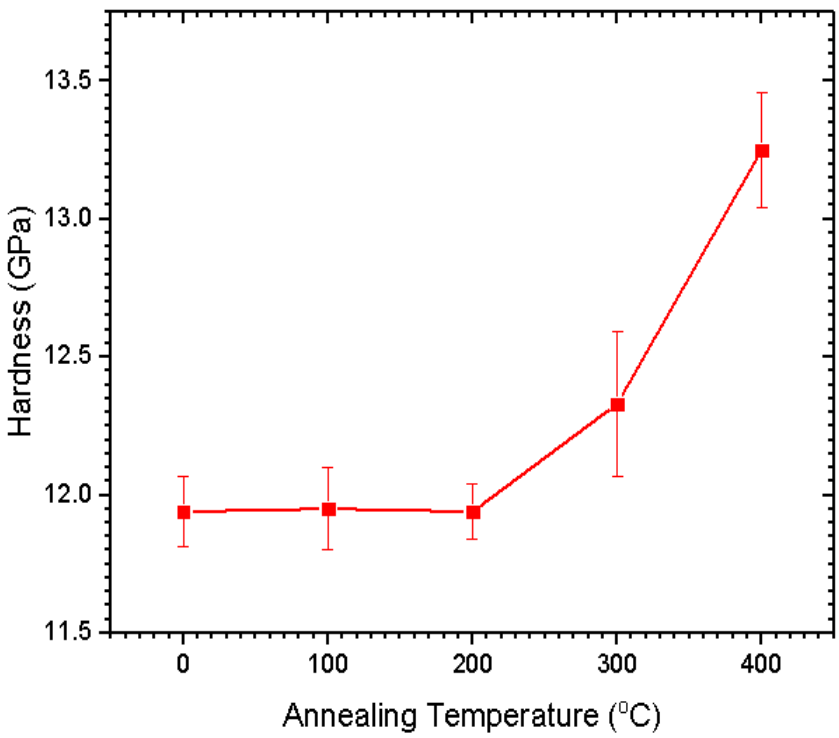

Figure 4.7: Graph of the hardness of the MG against annealing temperature

4.3.1.3 Effect of Size on the Hardness of the Metallic Glass

From the micrograph in Figure 4.2, it can clearly be seen that the metallic glass fractured inhomogeneously, producing fragments of varying sizes. The effect of the various sizes on the hardness of the metallic glass was investigated in this section. Seven different sizes were investigated and the results are shown in table 4.1 below. It was observed that the properties of the metallic glass in the Cu/MG system is independent of size.

Despite the fact that researchers have observed some size-dependent properties on the metallic glass as reviewed in section 2.2.4, the metallic glass presented in this investigation did not have

such size effects. This may be due to the fact that the metallic glass has not been broken down into the critical size in which size-dependent properties begin to occur.

Table 4.1: Hardness and elastic modulus properties due to the size of the metallic glass

Size (μm)	Hardness (GPa)
22.35	12.76 ± 0.13
17.56	12.69 ± 0.15
12.29	12.75 ± 0.13
10.91	12.76 ± 0.14
6.71	12.73 ± 0.11
5.48	12.71 ± 0.16
4.69	12.76 ± 0.15

4.3.2 Elastic Modulus

The elastic modulus is a measure of the material's stiffness. It is the slope of the elastic region of a stress-strain curve.

4.3.2.1 Effect of Strain on the Elastic Modulus of Metallic Glass

Figure 4.8 shows a plot of elastic modulus of the metallic glass against a number of ARB cycles. It was observed that as the number of ARB cycles increased, so did the elastic modulus of the

metallic glass. As in section 4.3.1.1, it is also important to note that intermediate heat treatment was not applied after each ARB cycle. The increase in the elastic modulus may be due to the new phase of nanocrystals that are formed within the shear bands. It has been reported that formation of nanocrystals increases atomic bonding energy [158]. Since atomic bonds are stronger, there is more resistance to elastic deformation. As deformation increases, the number of shear bands produced in the metallic glass also increases. The increase in the shear bands possibly led to an increase in the number of nanocrystals formed in the metallic glass and this in turn led to an increase in the elastic modulus.

The increase in elastic modulus may also be due to the structural changes that occur as a result of structural relaxation. Structural relaxation leads to stronger atomic bonds. These stronger atomic bonds lead to an improved resistance to elastic deformation, therefore increasing the elastic modulus.

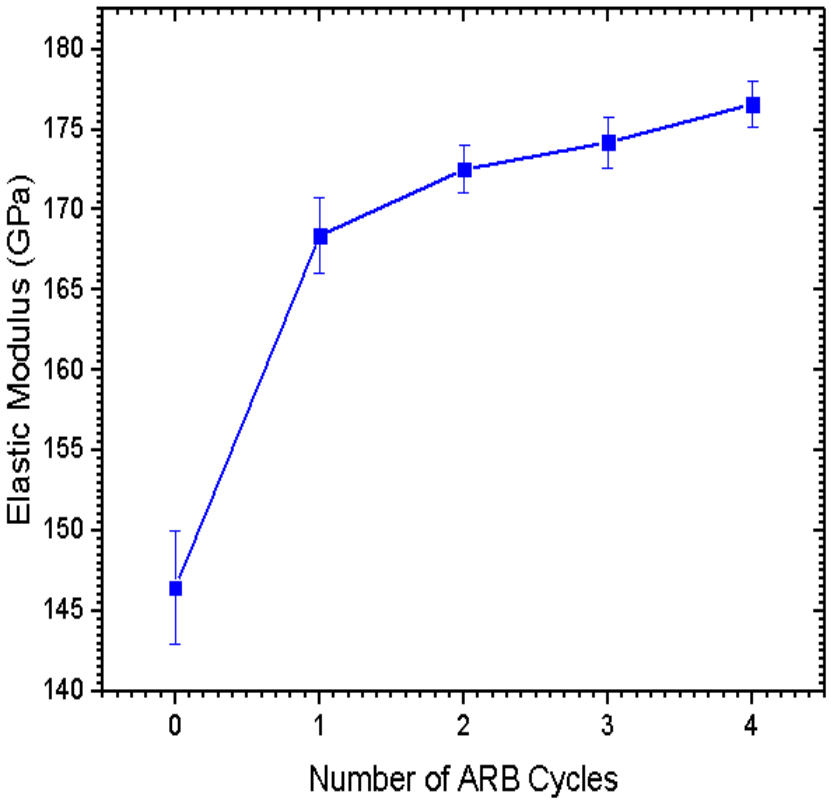

Figure 4.8: Graph of the elastic modulus of the MG against number of ARB cycles

4.3.2.2 Effect of Heat Treatment on the Elastic Modulus of Metallic Glass

Figure 4.9 shows a plot of elastic modulus against annealing temperature. Similar to what was observed with the hardness of the metallic glass as a result of annealing temperature, the elastic modulus also increased. Because of structural relaxation, free volume is reduced, atoms are now more densely packed, atoms have a higher atomic bonding energy and the metallic glass is now more resistant to elastic deformation and is now stiffer.

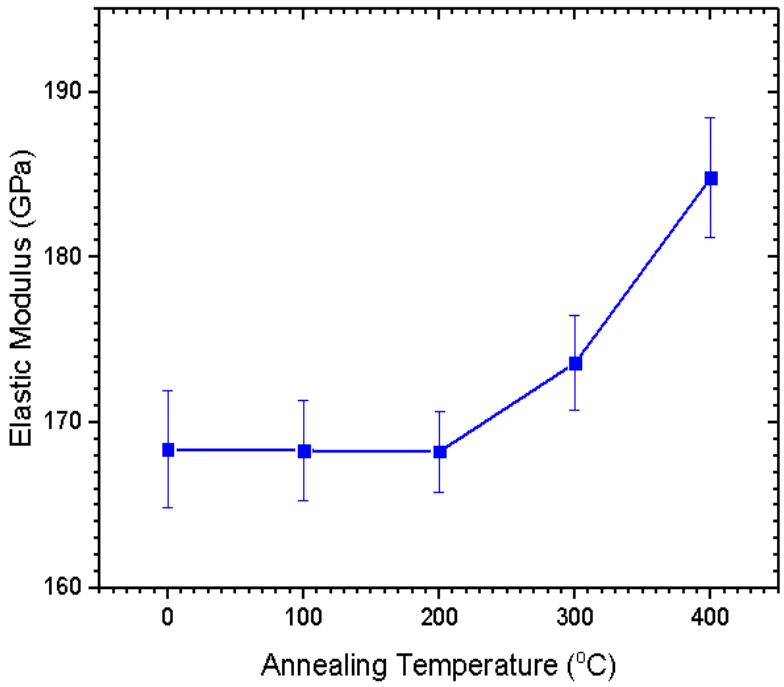

Figure 4.9: Graph of the elastic modulus of the MG against annealing temperature

4.3.2.3 Effect of Size on the Elastic Modulus of Metallic Glass

Similar results were observed in the elastic modulus measurements as in the hardness measurements. The elastic modulus property remained unchanged as a function of size. This could also be due to the fact that the sizes of the metallic glass did not reach the critical value where size effects can be observed. These results are shown in table 4.2.

Table 4.2: Elastic modulus properties due to the size of the metallic glass

Size (μm)	Elastic Modulus (GPa)
22.35	176.58 ± 1.39
17.56	176.55 ± 1.46
12.29	176.56 ± 1.37
10.91	176.59 ± 1.54
6.71	176.51 ± 1.87
5.48	176.40 ± 1.42
4.69	176.62 ± 1.23

4.3.3 Load-Displacement Curves

The load-displacement curves of the metallic glass in the Cu/MG system were investigated for "pop-ins". These "pop-ins" signify the onset of plastic deformation in amorphous materials in the load-displacement curves. Figures 4.10 and 4.11 show the load-displacement curves during nanoindentation for the as-received metallic glass and the Cu/MG system after four ARB cycles respectively. As it can be observed, "pop-ins" were generated during nanoindentation of both the as-received sample and the deformed sample. This is a strong indication that the metallic glass still possesses its amorphous characteristics.

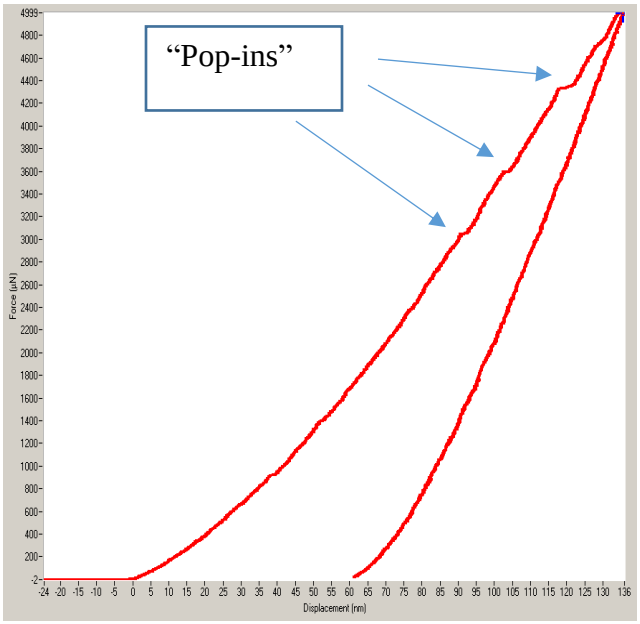

Figure 4.10: Load-displacement curve after nanoindentation of the as-received MG

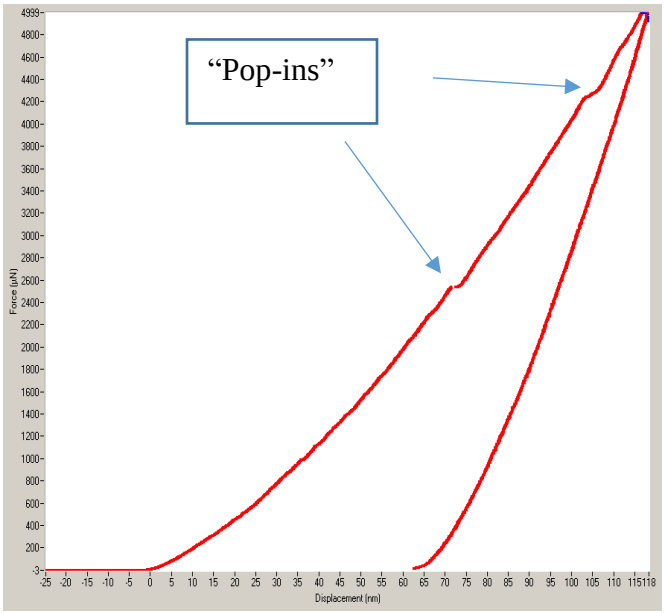

Figure 4.11: Load-displacement curve after nanoindentation of the MG after the fourth pass

Even though the heat treatment was done below the crystallization temperature of the metallic glass, load-displacement curves were still observed to investigate the amorphous structure of the metallic glass. Figure 4.12 shows the load-displacement curve of the sample annealed at 400 ^{o}C. “Pop-ins” can be observed in the curve indicating that the annealed sample still maintained its amorphous structure.

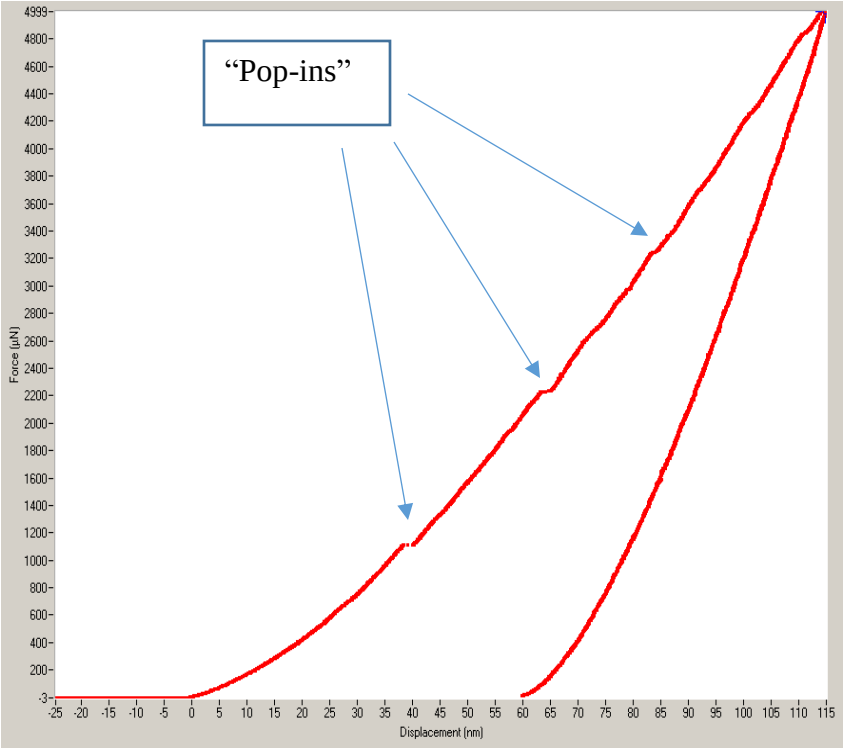

Figure 4.12: Load-displacement curve after nanoindentation of the MG after annealing at 400 ^{o}C

4.4 DSC Measurements

The DSC measurements were performed to determine if the crystallization temperature of the metallic glass was changed due to the strain imposed during ARB. Figures 4.13 shows the plot of heat flow against the temperature of the Cu/MG system after the fourth ARB cycle. In comparison

with figure 4.6, it was observed that the strain imposed did not have an effect on the crystallization temperature of the metallic glass as both results indicated a crystallization temperature of ~505 ºC.

Also, a larger peak can be observed on the as-received plot because the mass of metallic glass used for the investigation was more in the as-received sample than in the Cu/MG sample.

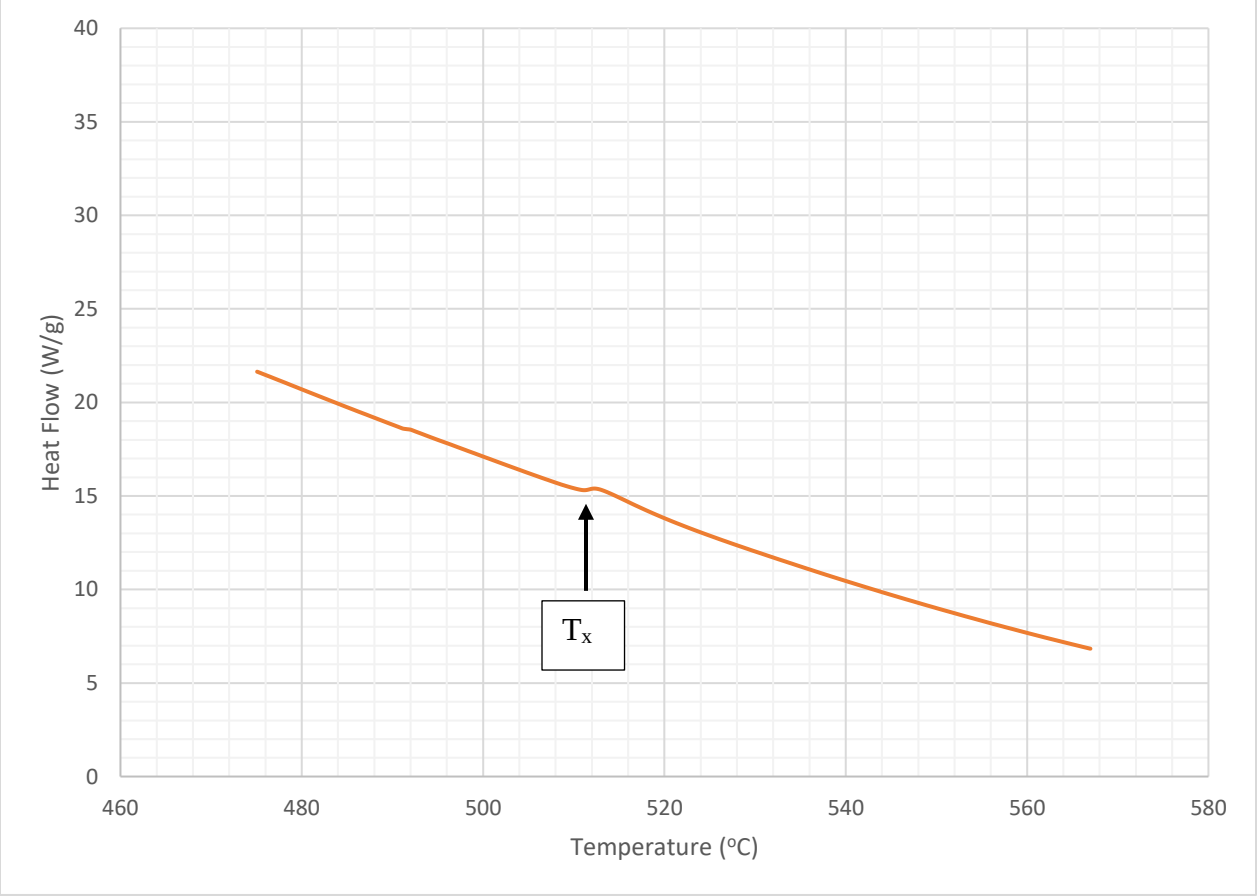

Figure 4.13: DSC plot indicating the crystallization temperature of the as-received metallic glass

4.5 Comparison between Heat Treatment of the Cu/MG and Ni/MG Systems

Cu/MG and Ni/MG systems were annealed at temperatures above the crystallization temperature of the metallic glass using the Carbolite Gero furnace. At temperatures between 700 and 800 ^{o}C, the microstructure of the "metallic glass" in the Cu/MG system remained unchanged, similar to the micrograph in figure 4.2. On the other hand, when the Ni/MG system was annealed at 800 ^{o}C, a structure was observed which could be due to melting and resolidification. Figure 4.14 shows the microstructure that was observed. Tiny particles of sizes ranging from 0.5 – 1 μm were seen.

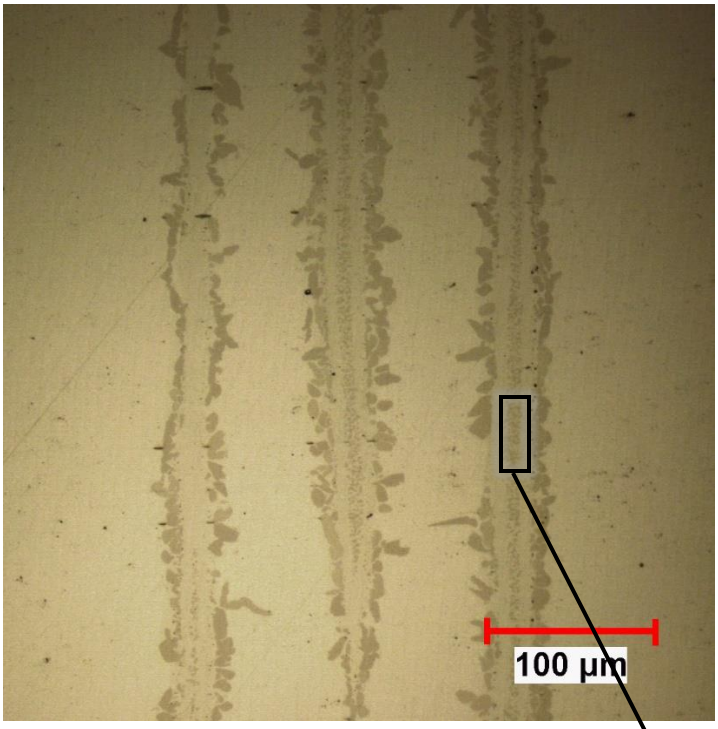

(a)

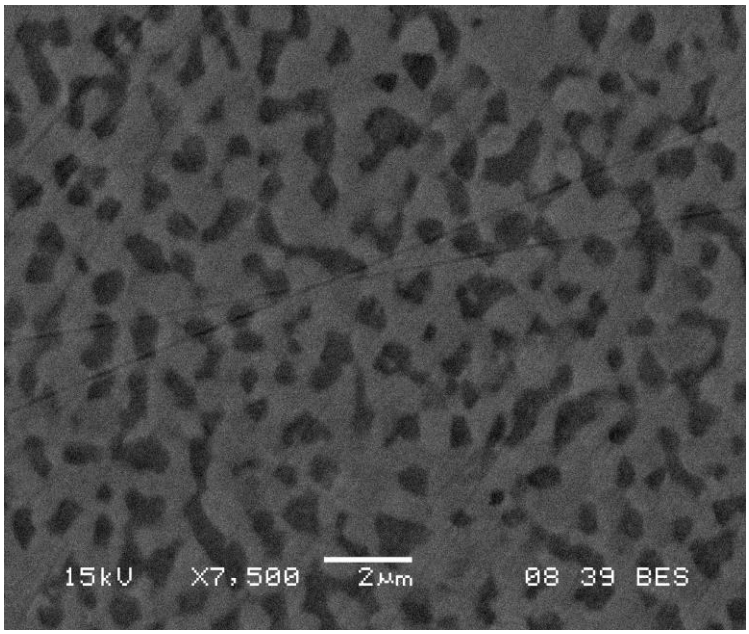

(b)

Figure 4.14: (a) Optical micrograph of the Ni/MG system annealed at 800 ^{o}C. (b) SEM image of the "melted metallic glass" region

A nanoindentation grid was performed from the base nickel region to the “melted metallic glass” region as shown in figure 4.15.

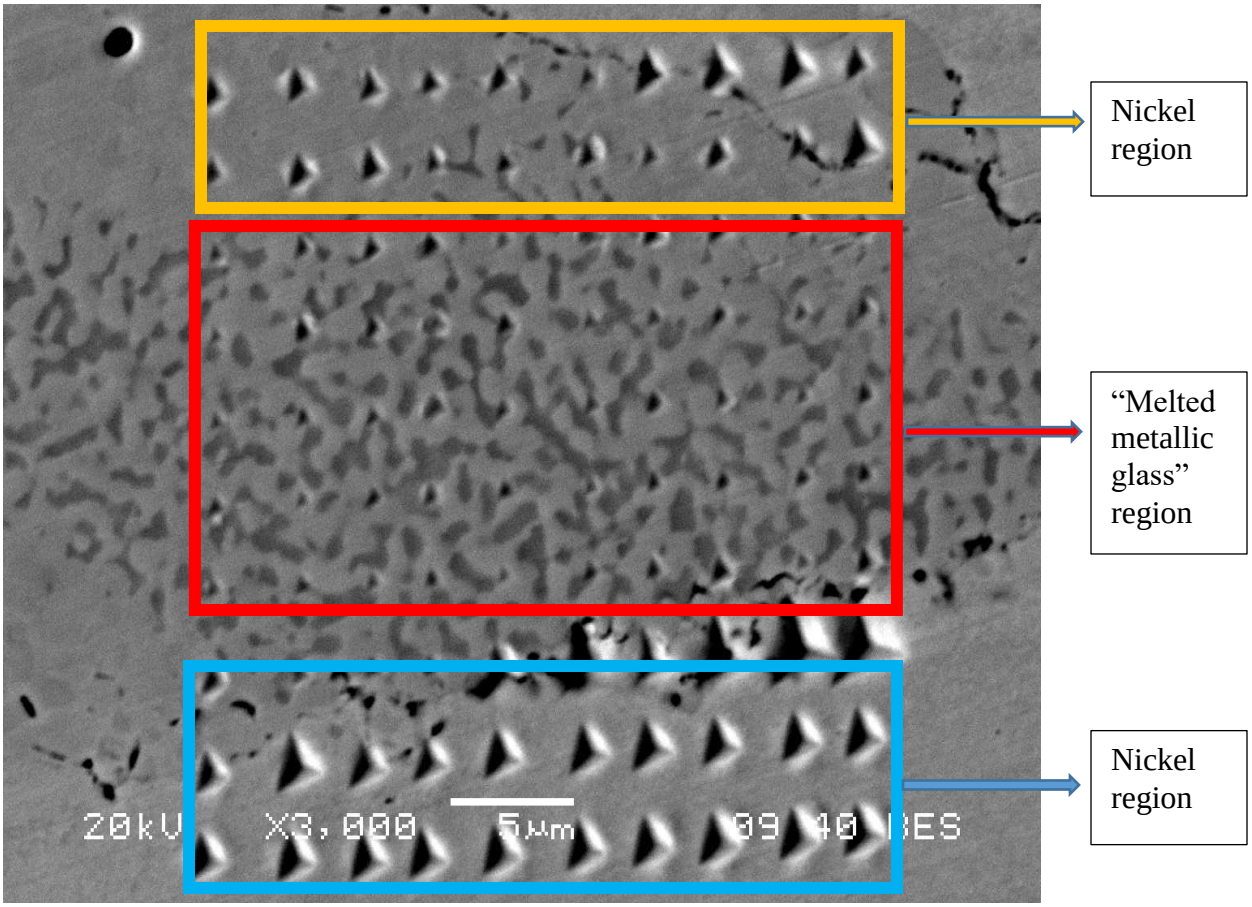

Figure 4.15: SEM image showing the nanoindentation grid from the nickel region to the “melted metallic glass region”

The grid shows an array of large indents along the nickel region to smaller indents along the “melted metallic glass” region. The results for the hardness and elastic modulus measurements are shown in Figures 4.16 and 4.17 respectively.

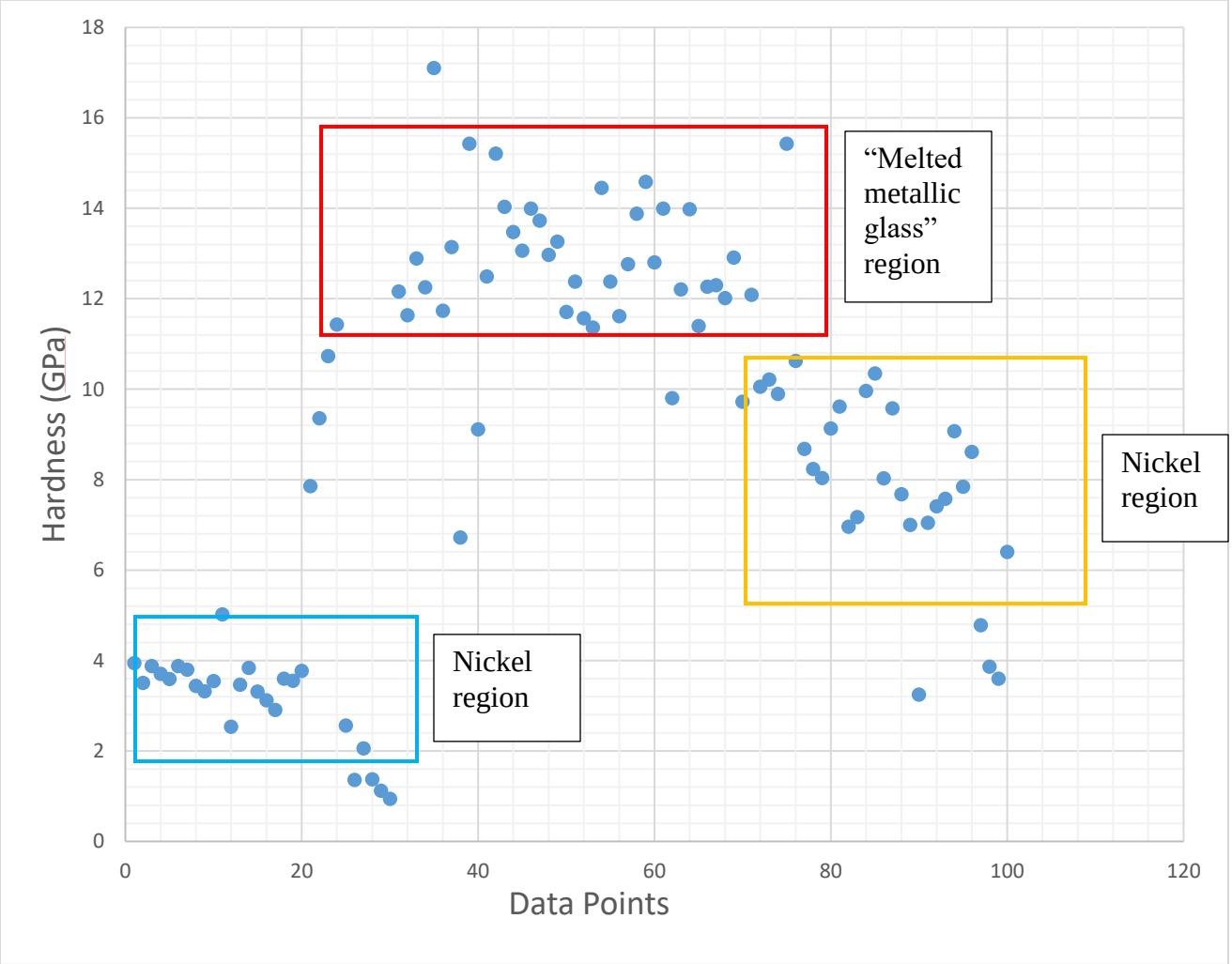

Figure 4.16: Graph illustrating the hardness variation for the three different regions

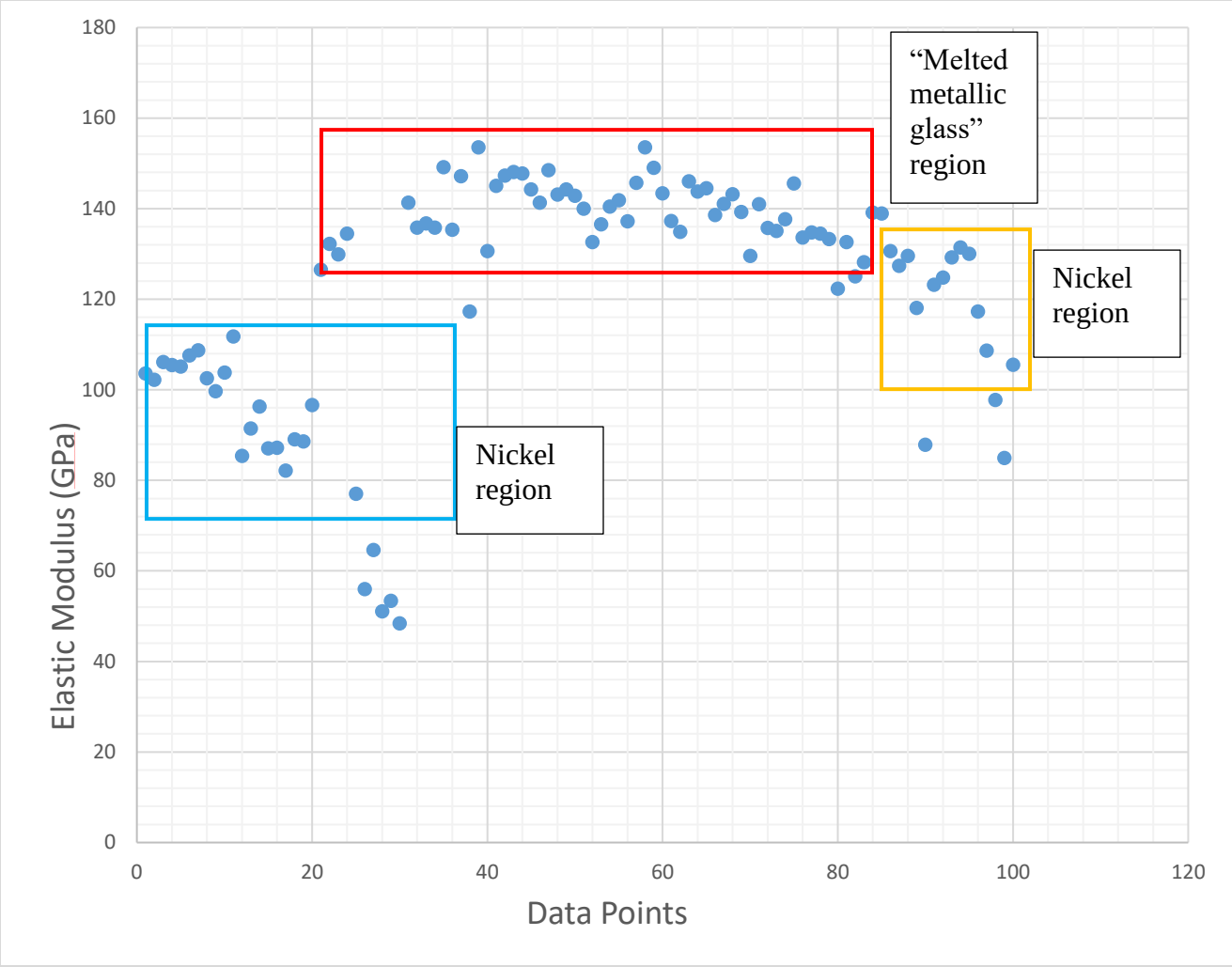

Figure 4.17: Graph illustrating the elastic modulus variation for the three different regions

The hardness and elastic modulus results reveal that the "melted metallic glass" region possesses superior properties compared to the as-received metallic glass. As nanoindentation progressed from the nickel region to the "melted metallic glass" region, hardness and elastic modulus properties began to increase. The points that are not represented on the graphs are outliers due to crack or error from the instrument. Experimental validation has not been conducted yet but these results may be due to the size of the particles.

Chapter 5 - Conclusions and Recommendations

5.1 Summary and Conclusions

The purpose of this research was to characterise a Ni-based metallic glass in a crystalline-amorphous composite by using a unique technique called nanoindentation. A study on the effect of ARB parameters such as strain and heat treatment on the metallic glass was also carried out. Lastly, the effect of size on the metallic glass investigated. The results from the experiments show that;

- ARB is an effective method for synthesizing the crystalline-amorphous composite as the materials used were bonded successfully even up to the fourth rolling cycle
- The brittle metallic glass fractured after the first cycle, and subsequent cycles led to the breaking of the metallic glass into the smaller fragment. These fragments are distributed in the copper matrix. However, the sizes of the fragments are uniform
- The EDS analysis suggests that there was no diffusion between the metallic glass and the copper materials at the boundary
- Nanoindentation of the samples was done using the Berkovich tip. The results revealed that the hardness and elastic modulus of the metallic glass increased as the number of ARB cycles increased. Apart from the increase in both the hardness and modulus, the results also showed that there were “pop-ins” in the load-displacement curve of the sample after the fourth ARB cycle. The presence of these pop-ins suggests that the metallic glass still maintained its amorphous structure even after deformation
- Nanoindentation results also showed that low-temperature heat treatment of 100 ^{o}C and 200 ^{o}C has no effect on the hardness and elastic modulus of the metallic glass. However,

when the metallic glass was annealed at 300 ^{o}C and 400 ^{o}C, the hardness and elastic modulus increased with increasing temperature. This revealed that there was possible structural relaxation as a result of the heat treatment. “Pop-ins” were also observed in the sample annealed at 400 ^{o}C, indicating the amorphous structure of the metallic glass

- The size effect of the metallic glass was also investigated and the results showed that the hardness and elastic modulus properties of the metallic glass does not depend on size
- While comparing the heat treatment of the Cu/MG and Ni/MG systems at 800 ^{o}C, it was observed that the melting of the metallic glass “metallic glass” likely occurred in the Ni/MG system while no melting was observed in the Cu/MG system.

In conclusion, the ARB process led to an increase in the hardness and modulus of the Ni-based metallic glass up to the fourth cycle. More ARB cycles led to a more homogenous distribution of the metallic glass in the crystalline matrix and no size effect was observed.

5.2 Recommendations for Future Works

- One of the main limitation of the research if the thickness of the metallic glass. If a metallic glass of larger thickness is used, there is a possibility of more homogeneous distribution of the metallic glass in the crystalline matrix
- Macroscopic tests such as tensile and compression tests were not carried out on the sample as a result of voids that were formed in copper during the ARB process. These voids serve as stress raisers. Warm rolling is a way to improve the ductility of copper and limit the formation of these voids. Warm rolling should be performed at between 300 and 400 ^{o}C as it improves bonding and also the properties of the metallic glass.

Bibliography

[1] A. Inoue, “Stabilization of metallic supercooled liquid and bulk amorphous alloys,” *Acta Mater.*, vol. 48, no. 1, pp. 279–306, 2000.

[2] E. Pekarskaya, J. F. Löffler, and W. L. Johnson, “Microstructural studies of crystallization of a Zr-based bulk metallic glass,” *Acta Mater.*, vol. 51, no. 14, pp. 4045–4057, 2003.

[3] J. F. Löffler, “Bulk metallic glasses,” *Intermetallics*, vol. 11, no. 6, pp. 529–540, 2003.

[4] A. . Argon, “Plastic deformation in metallic glasses,” *Acta Metall.*, vol. 27, no. 1, pp. 47–58, 1979.

[5] C. C. Hays, C. P. Kim, and W. L. Johnson, “Microstructure controlled shear band pattern formation and enhanced plasticity of bulk metallic glasses containing in situ formed ductile phase dendrite dispersions,” *Phys. Rev. Lett.*, vol. 84, no. 13, pp. 2901–2904, 2000.

[6] T. Kozieł, Z. Kedzierski, A. Zielińska-Lipiec, and K. Ziewiec, “The microstructure of liquid immiscible Fe-Cu-based in situ formed amorphous/crystalline composite,” *Scr. Mater.*, vol. 54, no. 12, pp. 1991–1995, 2006.

[7] Q. Su, L. Price, J. A. Colon Santana, L. Shao, and M. Nastasi, “Irradiation tolerance of amorphous SiOC/crystalline Fe composite,” *Mater. Lett.*, vol. 155, pp. 138–141, 2015.

[8] H. Sieber, G. Wilde, and J. H. Perepezko, “Thermally activated amorphous phase formation in cold-rolled multilayers of Al ± Ni , Al ± Ta , Al ± Fe and Zr ± Cu,” vol. 252, pp. 611–615, 1999.

[9] W. Callister and D. Rethwisch, *Materials science and engineering: an introduction*, vol. 94. 2007.

[10] D. M. Poojary and A. Clearfield, “Application of X-ray Powder Diffraction Techniques to the Solution of Unknown Crystal Structures,” *Acc. Chem. Res.*, vol. 30, no. 10, pp. 414–422, 1997.

[11] E. O. Hall, “the Deformation and Ageing of Mild Steel .3. Discussion of Results,” *Proc. Phys. Soc. London Sect. B*, vol. 64, no. 381, pp. 747–753, 1951.

[12] P. N.J, “The Cleavage Strength of Polycrystals,” *J. Iron Steel Inst.*, vol. 174, p. 1982, 1953.

[13] A. S. M. Agena, “A study of flow characteristics of nanostructured Al-6082 alloy produced by ECAP under upsetting test,” *J. Mater. Process. Technol.*, vol. 209, no. 2, pp. 856–863, 2009.

[14] M. Ke, S. A. Hackney, W. W. Milligan, and E. C. Aifantis, “Observation and measurement of grain rotation and plastic strain in nanostructured metal thin films,” *Nanostructured Mater.*, vol. 5, no. 6, pp. 689–697, 1995.

[15] Y. B. Wang, B. Q. Li, M. L. Sui, and S. X. Mao, “Deformation-induced grain rotation and growth in nanocrystalline Ni,” *Appl. Phys. Lett.*, vol. 92, no. 1, pp. 2006–2009, 2008.

[16] D. Farkas, S. Mohanty, and J. Monk, “Strain-driven grain boundary motion in

nanocrystalline materials," *Mater. Sci. Eng. A*, vol. 493, no. 1–2, pp. 33–40, 2008.

[17] H. Van Swygenhoven and P. M. Derlet, "Grain-boundary sliding in nanocrystalline fcc metals," *Phys. Rev. B - Condens. Matter Mater. Phys.*, vol. 64, no. 22, pp. 1–9, 2001.

[18] M. Legros, D. S. Gianola, and K. J. Hemker, "In situ TEM observations of fast grain-boundary motion in stressed nanocrystalline aluminum films," *Acta Mater.*, vol. 56, no. 14, pp. 3380–3393, 2008.

[19] D. S. Gianola, C. Eben, X. Cheng, and K. J. Hemker, "Stress-driven surface topography evolution in nanocrystalline al thin films," *Adv. Mater.*, vol. 20, no. 2, pp. 303–308, 2008.

[20] D. S. Gianola, S. Van Petegem, M. Legros, S. Brandstetter, H. Van Swygenhoven, and K. J. Hemker, "Stress-assisted discontinuous grain growth and its effect on the deformation behavior of nanocrystalline aluminum thin films," *Acta Mater.*, vol. 54, no. 8, pp. 2253–2263, 2006.

[21] D. Kiener, C. Motz, and G. Dehm, "Micro-compression testing: A critical discussion of experimental constraints," *Mater. Sci. Eng. A*, vol. 505, no. 1–2, pp. 79–87, 2009.

[22] A. T. Jennings, M. J. Burek, and J. R. Greer, "Microstructure versus Size: Mechanical properties of electroplated single crystalline Cu nanopillars," *Phys. Rev. Lett.*, vol. 104, no. 13, pp. 1–4, 2010.

[23] J. R. Greer and W. D. Nix, "Nanoscale gold pillars strengthened through dislocation starvation," *Phys. Rev. B - Condens. Matter Mater. Phys.*, vol. 73, no. 24, pp. 1–6, 2006.

[24] A. S. Budiman, S. M. Han, J. R. Greer, N. Tamura, J. R. Patel, and W. D. Nix, "A search for evidence of strain gradient hardening in Au submicron pillars under uniaxial compression using synchrotron X-ray microdiffraction," *Acta Mater.*, vol. 56, no. 3, pp. 602–608, 2008.

[25] K. S. Ng and A. H. W. Ngan, "Breakdown of Schmid's law in micropillars," *Scr. Mater.*, vol. 59, no. 7, pp. 796–799, 2008.

[26] S. H. Oh, M. Legros, D. Kiener, and G. Dehm, "In situ observation of dislocation nucleation and escape in a submicrometre aluminium single crystal," *Nat. Mater.*, vol. 8, no. 2, pp. 95–100, 2009.

[27] Z. W. Shan, R. K. Mishra, S. A. Syed Asif, O. L. Warren, and A. M. Minor, "Mechanical annealing and source-limited deformation in submicrometre- diameter Nicrystals," *Nat. Mater.*, vol. 7, no. 2, pp. 115–119, 2008.

[28] C. P. Frick, B. G. Clark, S. Orso, A. S. Schneider, and E. Arzt, "Size effect on strength and strain hardening of small-scale [1 1 1] nickel compression pillars," *Mater. Sci. Eng. A*, vol. 489, no. 1–2, pp. 319–329, 2008.

[29] D. Jang and J. R. Greer, "Size-induced weakening and grain boundary-assisted deformation in 60 nm grained Ni nanopillars," *Scr. Mater.*, vol. 64, no. 1, pp. 77–80, 2011.

[30] A. Rinaldi, P. Peralta, C. Friesen, and K. Sieradzki, "Sample-size effects in the yield behavior of nanocrystalline nickel," *Acta Mater.*, vol. 56, no. 3, pp. 511–517, 2008.

[31] W. D. Nix, J. R. Greer, G. Feng, and E. T. Lilleodden, “Deformation at the nanometer and micrometer length scales: Effects of strain gradients and dislocation starvation,” *Thin Solid Films*, vol. 515, no. 6, pp. 3152–3157, 2007.

[32] J. R. Greer, W. C. Oliver, and W. D. Nix, “Size dependence of mechanical properties of gold at the micron scale in the absence of strain gradients,” *Acta Mater.*, vol. 53, no. 6, pp. 1821–1830, 2005.

[33] M. D. Uchic, D. M. Dimiduk, J. N. Florando, and W. D. Nix, “Sample Dimension Influence Strength and Crystal Plasticity,” *Science (80-.).*, vol. 305, no. August, pp. 986–989, 2004.

[34] M. D. Uchic and D. M. Dimiduk, “A methodology to investigate size scale effects in crystalline plasticity using uniaxial compression testing,” *Mater. Sci. Eng. A*, vol. 400–401, no. 1–2 SUPPL., pp. 268–278, 2005.

[35] M. Telford, “The case for bulk metallic glass,” *Mater. Today*, vol. 7, no. 3, pp. 36–43, 2004.

[36] L. Zhang, M. J. Zhuo, and J. Xu, “Enhancing bulk metallic glass formation in Ni-Nb-Sn-based alloys via substitutional alloying with Co and Hf,” *J. Mater. Res.*, vol. 23, no. 3, pp. 688–699, 2008.

[37] A. Peker and W. L. Johnson, “A highly processable metallic glass: Zr41.2Ti13.8Cu12.5Ni10.0Be22.5,” *Appl. Phys. Lett.*, vol. 63, no. 17, pp. 2342–2344, 1993.

[38] H. B. Lou, X. D. Wang, F. Xu, S. Q. Ding, Q. P. Cao, K. Hono, and J. Z. Jiang, “73 Mm-Diameter Bulk Metallic Glass Rod By Copper Mould Casting,” *Appl. Phys. Lett.*, vol. 99, no. 5, 2011.

[39] N. N. and H. K. Akihisa Inoue, “Preparation and Thermal Stability of Bulk Amorphous Pd40Cu30Ni10P20 Alloy Cylinder of 72 mm in Diameter,” *Mater. Trans.*, vol. 38, no. 2, p. 179 to 183, 1997.

[40] N. Nishiyama, K. Takenaka, H. Miura, N. Saidoh, Y. Zeng, and A. Inoue, “The world’s biggest glassy alloy ever made,” *Intermetallics*, vol. 30, pp. 19–24, 2012.

[41] H. Men, S. J. Pang, and T. Zhang, “Effect of Er doping on glass-forming ability of Co50 Cr15 Mo14 C15B6 alloy,” *J. Mater. Res.*, vol. 21, no. 4, pp. 958–961, 2006.

[42] E. S. Park and D. H. Kim, “Phase separation and enhancement of plasticity in Cu – Zr – Al – Y bulk metallic glasses,” vol. 54, pp. 2597–2604, 2006.

[43] Y. Shen, E. Ma, and J. Xu, “A group of Cu (Zr)-based BMGs with critical diameter in the range of 12 to 18 mm,” *J. Mater. Sci. …*, vol. 24, no. 2, pp. 149–152, 2008.

[44] J. Schroers, B. Lohwongwatana, W. L. Johnson, and A. Peker, “Gold based bulk metallic glass,” *Appl. Phys. Lett.*, vol. 87, no. 6, pp. 1–4, 2005.

[45] Q. K. Jiang, G. Q. Zhang, L. Yang, X. D. Wang, K. Saksl, H. Franz, R. Wunderlich, H. Fecht, and J. Z. Jiang, “La-based bulk metallic glasses with critical diameter up to 30 mm,” *Acta Mater.*, vol. 55, no. 13, pp. 4409–4418, 2007.

[46] J. Pan, Q. Chen, N. Li, and L. Liu, “Formation of centimeter Fe-based bulk metallic glasses

in low vacuum environment," *J. Alloys Compd.*, vol. 463, no. 1–2, pp. 246–249, 2008.

[47] Q. Zheng, J. Xu, and E. Ma, "High glass-forming ability correlated with fragility of Mg-Cu(Ag)-Gd alloys," *J. Appl. Phys.*, vol. 102, no. 11, pp. 1–6, 2007.

[48] F. Guo, H. J. Wang, S. J. Poon, and G. J. Shiflet, "Ductile titanium-based glassy alloy ingots," *Appl. Phys. Lett.*, vol. 86, no. 9, pp. 1–3, 2005.

[49] L. Zhang, E. Ma, and J. Xu, "Hf-based bulk metallic glasses with critical diameter on centimeter scale," *Intermetallics*, vol. 16, no. 4, pp. 584–586, 2008.

[50] B. Zhang, D. Q. Zhao, M. X. Pan, R. J. Wang, and W. H. Wang, "Formation of cerium-based bulk metallic glasses," *Acta Mater.*, vol. 54, no. 11, pp. 3025–3032, 2006.

[51] J. X. Li, G. B. Shan, K. W. Gao, L. J. Qiao, and W. Y. Chu, "In situ SEM study of formation and growth of shear bands and microcracks in bulk metallic glasses," *Mater. Sci. Eng. A*, vol. 354, no. 1–2, pp. 337–343, 2003.

[52] A. C. Lund and C. A. Schuh, "The Mohr-Coulomb criterion from unit shear processes in metallic glass," *Intermetallics*, vol. 12, no. 10–11 SPEC. ISS., pp. 1159–1165, 2004.

[53] P. E. Donovan, "Compressive deformation of amorphous $Pd_{40}Ni_{40}P_{20}$," *Mater. Sci. Eng.*, vol. 98, pp. 487–490, 1988.

[54] H. Chen, Y. He, G. J. Shiflet, and S. J. Poon, "Deformation-induced nanocrystal formation in shear bands of amorphous alloys," *Nature*, vol. 367, no. 6463, pp. 541–543, 1994.

[55] J. Li, F. Spaepen, and T. C. Hufnagel, "Nanometre-scale defects in shear bands in a metallic glass," *Philos. Mag. A Phys. Condens. Matter, Struct. Defects Mech. Prop.*, vol. 82, no. 13, pp. 2623–2630, 2002.

[56] Z. F. Zhang, J. Eckert, and L. Schultz, "Difference in compressive and tensile fracture mechanisms of Zr59Cu20Al10Ni8Ti3bulk metallic glass," *Acta Mater.*, vol. 51, no. 4, pp. 1167–1179, 2003.

[57] F. Spaepen, "On the fracture morphology of metallic glasses," *Acta Metall.*, vol. 23, no. 5, pp. 615–620, 1975.

[58] W. J. Wright, R. B. Schwarz, and W. D. Nix, "Localized heating during serrated plastic flow in bulk metallic glasses," *Mater. Sci. Eng. A*, vol. 319–321, pp. 229–232, 2001.

[59] P. H. Gaskell, "Glassy Metals II," pp. 5–49, 1983.

[60] T. Masumoto and R. Maddin, "Structural stability and mechanical properties of amorphous metals," *Mater. Sci. Eng.*, vol. 19, no. 1, pp. 1–24, 1975.

[61] F. Szuecs, C. P. Kim, and W. L. Johnson, "DUCTILE PHASE REINFORCED BULK METALLIC GLASS COMPOSITE," vol. 49, pp. 1507–1513, 2001.

[62] J. W. Qiao, S. Wang, Y. Zhang, P. K. Liaw, and G. L. Chen, "Large plasticity and tensile necking of Zr-based bulk-metallic-glass-matrix composites synthesized by the Bridgman solidification," *Appl. Phys. Lett.*, vol. 94, no. 15, pp. 0–3, 2009.

[63] J. W. Qiao, A. C. Sun, E. W. Huang, Y. Zhang, P. K. Liaw, and C. P. Chuang, "Tensile

deformation micromechanisms for bulk metallic glass matrix composites: From work-hardening to softening," *Acta Mater.*, vol. 59, no. 10, pp. 4126–4137, 2011.

[64] Y. Zhang, W. Xu, H. Tan, and Y. Li, "Microstructure control and ductility improvement of La-Al-(Cu, Ni) composites by Bridgman solidification," *Acta Mater.*, vol. 53, no. 9, pp. 2607–2616, 2005.

[65] L. and A. I. Fan, Cang, Chunfei, "Deformation behaviour of Zr-based bulk nanocrystalline amorphous alloys," *Phys. Rev. B - Condens. Matter Mater. Phys.*, vol. 61, no. 6, pp. 3761–3763, 2000.

[66] J. Fornell, E. Rossinyol, S. Suriñach, M. D. Baró, W. H. Li, and J. Sort, "Enhanced mechanical properties in a Zr-based metallic glass caused by deformation-induced nanocrystallization," *Scr. Mater.*, vol. 62, no. 1, pp. 13–16, 2010.

[67] K. Wang, T. Fujita, Y. Q. Zeng, N. Nishiyama, A. Inoue, and M. W. Chen, "Micromechanisms of serrated flow in a Ni50Pd30P20bulk metallic glass with a large compression plasticity," *Acta Mater.*, vol. 56, no. 12, pp. 2834–2842, 2008.

[68] J.-J. Kim, Y. Choi, S. Suresh, and A. S. Argon, "Nanocrystallization During Nanoindentation of a Bulk Amorphous Metal Alloy at Room Temperature," *Science (80-.).*, vol. 295, no. 5555, pp. 654–657, 2002.

[69] Z. T. Wang, J. Pan, Y. Li, and C. A. Schuh, "Densification and strain hardening of a metallic glass under tension at room temperature," *Phys. Rev. Lett.*, vol. 111, no. 13, pp. 1–5, 2013.

[70] C. E. Packard, L. M. Witmer, and C. A. Schuh, "Hardening of a metallic glass during cyclic loading in the elastic range," *Appl. Phys. Lett.*, vol. 92, no. 17, 2008.

[71] P. W. Bridgman and I. Šimon, "Effects of very high pressures on glass," *J. Appl. Phys.*, vol. 24, no. 4, pp. 405–413, 1953.

[72] T. Rouxel, H. Ji, T. Hammouda, and A. Moréac, "Poisson's ratio and the densification of glass under high pressure," *Phys. Rev. Lett.*, vol. 100, no. 22, pp. 1–4, 2008.

[73] A. D. Drozdov, "Stress-induced densification of glassy polymers in the subyield region," *J. Appl. Polym. Sci.*, vol. 74, no. 7, pp. 1705–1718, 1999.

[74] V. V. Khonik, V.A., Kosilov, A.T., Mikhailov, V.A., Sviridov, "Isothermal creep of metallic glasses: a new approach and its experimental verification," *Acta Mater.*, vol. 46, no. 10, pp. 3399–3408, 1998.

[75] T. Egami, "Structural Relaxation in Metallic Glasses," *Ann. N. Y. Acad. Sci.*, vol. 371, no. 1, pp. 238–251, 1981.

[76] A. Inoue, T. Zhang, and T. Masumoto, "the Structural Relaxation and Glass-Transition of La-Al-Ni and Zr-Al-Cu Amorphous-Alloys With a Significant Supercooled Liquid Region," *J. Non. Cryst. Solids*, vol. 150, no. 1–3, pp. 396–400, 1992.

[77] A. Slipenyuk and J. Eckert, "Correlation between enthalpy change and free volume reduction during structural relaxation of Zr55Cu30Al10Ni5metallic glass," *Scr. Mater.*, vol. 50, no. 1, pp. 39–44, 2004.

[78] Y. X. Zhuang and W. H. Wang, “Effects of relaxation on glass transition and crystallization of ZrTiCuNiBe bulk metallic glass,” *J. Appl. Phys.*, vol. 87, no. 11, pp. 8209–8211, 2000.

[79] U. Ramamurty, M. L. Lee, J. Basu, and Y. Li, “Embrittlement of a bulk metallic glass due to low-temperature annealing,” *Scr. Mater.*, vol. 47, no. 2, pp. 107–111, 2002.

[80] X. L. Wang, J. Almer, C. T. Liu, Y. D. Wang, J. K. Zhao, A. D. Stoica, D. R. Haeffner, and W. H. Wang, “In situ synchrotron study of phase transformation behaviors in bulk metallic glass by simultaneous diffraction and small angle scattering,” *Phys. Rev. Lett.*, vol. 91, no. 26, pp. 24–27, 2003.

[81] W. Dmowski, C. Fan, M. L. Morrison, P. K. Liaw, and T. Egami, “Structural changes in bulk metallic glass after annealing below the glass-transition temperature,” *Mater. Sci. Eng. A*, vol. 471, no. 1–2, pp. 125–129, 2007.

[82] C. A. Schuh, A. C. Lund, and T. G. Nieh, “New regime of homogeneous flow in the deformation map of metallic glasses: Elevated temperature nanoindentation experiments and mechanistic modeling,” *Acta Mater.*, vol. 52, no. 20, pp. 5879–5891, 2004.

[83] C. A. Schuh, T. C. Hufnagel, and U. Ramamurty, “Mechanical behavior of amorphous alloys,” *Acta Mater.*, vol. 55, no. 12, pp. 4067–4109, 2007.

[84] Q. Zheng, S. Cheng, J. H. Strader, E. Ma, and J. Xu, “Critical size and strength of the best bulk metallic glass former in the Mg – Cu – Gd ternary system Critical size and strength of the best bulk metallic glass former in the Mg – Cu – Gd ternary system,” no. January, 2007.

[85] H. Guo, P. F. Yan, Y. B. Wang, J. Tan, Z. F. Zhang, M. L. Sui, and E. Ma, “Tensile ductility and necking of metallic glass.,” *Nat. Mater.*, vol. 6, no. 10, pp. 735–739, 2007.

[86] D. Jang and J. R. Greer, “Transition from a strong-yet-brittle to a stronger-and-ductile state by size reduction of metallic glasses,” *Nat. Mater.*, vol. 9, no. 3, pp. 215–219, 2010.

[87] F. F. Wu, Z. F. Zhang, and S. X. Mao, “Size-dependent shear fracture and global tensile plasticity of metallic glasses,” *Acta Mater.*, vol. 57, no. 1, pp. 257–266, 2009.

[88] X. J. Gu, S. J. Poon, G. J. Shiflet, and J. J. Lewandowski, “Compressive plasticity and toughness of a Ti-based bulk metallic glass,” *Acta Mater.*, vol. 58, no. 5, pp. 1708–1720, 2010.

[89] C. A. Volkert, A. Donohue, and F. Spaepen, “Effect of sample size on deformation in amorphous metals,” *J. Appl. Phys.*, vol. 103, no. 8, 2008.

[90] Q. Zheng, S. Cheng, J. H. Strader, E. Ma, and J. Xu, “Critical size and strength of the best bulk metallic glass former in the Mg-Cu-Gd ternary system,” *Scr. Mater.*, vol. 56, no. 2, pp. 161–164, 2007.

[91] Y. H. Lai, C. J. Lee, Y. T. Cheng, H. S. Chou, H. M. Chen, X. H. Du, C. I. Chang, J. C. Huang, S. R. Jian, J. S. C. Jang, and T. G. Nieh, “Bulk and microscale compressive behavior of a Zr-based metallic glass,” *Scr. Mater.*, vol. 58, no. 10, pp. 890–893, 2008.

[92] C. Q. Chen, Y. T. Pei, and J. T. M. De Hosson, “Effects of size on the mechanical response of metallic glasses investigated through in situ TEM bending and compression

experiments," *Acta Mater.*, vol. 58, no. 1, pp. 189–200, 2010.

[93] J. T. M. De Hosson, "Advances in transmission electron microscopy: In situ straining and in situ compression experiments on metallic glasses," *Microsc. Res. Tech.*, vol. 72, no. 3, pp. 250–260, 2009.

[94] A. Dubach, R. Raghavan, J. F. Löffler, J. Michler, and U. Ramamurty, "Micropillar compression studies on a bulk metallic glass in different structural states," *Scr. Mater.*, vol. 60, no. 7, pp. 567–570, 2009.

[95] X. H. Lin and W. L. Johnson, "Formation of Ti-Zr-Cu-Ni bulk metallic glasses," *J. Appl. Phys.*, vol. 78, no. 11, pp. 6514–6519, 1995.

[96] S. Pang, T. Zhang, K. Asami, and A. Inoue, "Synthesis of Fe–Cr–Mo–C–B–P bulk metallic glasses with high corrosion resistance," *Acta Mater.*, vol. 50, no. 3, pp. 489–497, 2002.

[97] A. Inoue, K. Ohtera, and T. Masumoto, "New amorphous al-y, al-la and al-ce alloys prepared by melt spinning," *Jpn. J. Appl. Phys.*, vol. 27, no. 5A, pp. L736–L739, 1988.

[98] D. Pavuna, "Production of metallic glass ribbons by the chill-block melt-spinning technique in stabilized laboratory conditions," *J. Mater. Sci.*, vol. 16, no. 9, pp. 2419–2433, 1981.

[99] A. Shelyakov, N. Sitnikov, S. Saakyan, A. Menushenkov, R. Rizakhanov, and A. Korneev, "Study of Two-Way Shape Memory Behavior of Amorphous-Crystalline TiNiCu Melt-Spun Ribbons," *Mater. Sci. Forum*, vol. 738–739, no. January 2013, pp. 352–356, 2013.

[100] T. Kozieł, J. Latuch, and A. Zielińska-Lipiec, "Structure of the amorphous-crystalline Fe66Cu6B19Si5Nb4alloy obtained by the melt-spinning process," *Arch. Metall. Mater.*, vol. 58, no. 2, pp. 601–605, 2013.

[101] K. Ziewiec and Z. Kedzierski, "The microstructure development in Fe32Cu20Ni28P10Si5B5 immiscible alloy and possibilities of formation of amorphous/crystalline composite," *J. Alloys Compd.*, vol. 480, no. 2, pp. 306–310, 2009.

[102] A. V. Shelyakov, N. N. Sitnikov, A. P. Menushenkov, A. A. Korneev, R. N. Rizakhanov, and N. A. Sokolova, "Fabrication and characterization of amorphous-crystalline TiNiCu melt-spun ribbons," *J. Alloys Compd.*, vol. 577, no. SUPPL. 1, pp. S251–S254, 2013.

[103] A. K. Jassim and A. S. Hammood, "Sustainable Manufacturing Process for Bulk Metallic Glasses Production Using Rapid Solidification with Melt Spinning Technique," no. Msme, 2014.

[104] G. He, W. Löser, and J. Eckert, "In situ formed Ti-Cu-Ni-Sn-Ta nanostructure-dendrite composite with large plasticity," *Acta Mater.*, vol. 51, no. 17, pp. 5223–5234, 2003.

[105] Y. Wang, J. Li, A. V. Hamza, and T. W. Barbee, "Ductile crystalline-amorphous nanolaminates," *Proc. Natl. Acad. Sci.*, vol. 104, no. 27, pp. 11155–11160, 2007.

[106] N. Nedfors, O. Tengstrand, A. Flink, P. Eklund, L. Hultman, and U. Jansson, "Characterization of amorphous and nanocomposite Nb-Si-C thin films deposited by DC magnetron sputtering," *Thin Solid Films*, vol. 545, pp. 272–278, 2013.

[107] N. Tsuji, Y. Saito, H. Utsunomiya, and S. Tanigawa, "Ultra-fine grained bulk steel produced

by accumulative roll-bonding (ARB) process," *Scr. Mater.*, vol. 40, no. 7, pp. 795–800, 1999.

[108] M. Eizadjou, A. Kazemi Talachi, H. Danesh Manesh, H. Shakur Shahabi, and K. Janghorban, "Investigation of structure and mechanical properties of multi-layered Al/Cu composite produced by accumulative roll bonding (ARB) process," *Compos. Sci. Technol.*, vol. 68, no. 9, pp. 2003–2009, 2008.

[109] A. Mozaffari, H. Danesh Manesh, and K. Janghorban, "Evaluation of mechanical properties and structure of multilayered Al/Ni composites produced by accumulative roll bonding (ARB) process," *J. Alloys Compd.*, vol. 489, no. 1, pp. 103–109, 2010.

[110] R. N. Dehsorkhi, F. Qods, and M. Tajally, "Investigation on microstructure and mechanical properties of Al-Zn composite during accumulative roll bonding (ARB) process," *Mater. Sci. Eng. A*, vol. 530, no. 1, pp. 63–72, 2011.

[111] M. Tayyebi and B. Eghbali, "Study on the microstructure and mechanical properties of multilayer Cu/Ni composite processed by accumulative roll bonding," *Mater. Sci. Eng. A*, vol. 559, pp. 759–764, 2013.

[112] P. J. Hsieh, Y. C. Lo, C. T. Wang, J. C. Huang, and S. P. Ju, "Cyclic transformation between nanocrystalline and amorphous phases in Zr based intermetallic alloys during ARB," *Intermetallics*, vol. 15, no. 5–6, pp. 644–651, 2007.

[113] Hidemi Kato and Akihisa Inoue, "Sysnthesis and Mechanical Properties of Bulk Amorphous Zr-Al-Ni-Cu Alloys Containing ZrC Particles," *Mater. Trans. JIM*, vol. 38, no. 9, p. 793 to 800, 1997.

[114] H. M. Fu, H. Wang, H. F. Zhang, and Z. Q. Hu, "In situ TiB-reinforced Cu-based bulk metallic glass composites," *Scr. Mater.*, vol. 54, no. 11, pp. 1961–1966, 2006.

[115] H. Choi-Yim and W. L. Johnson, "Bulk metallic glass matrix composites," *Appl. Phys. Lett.*, vol. 71, no. 26, pp. 3808–3810, 1997.

[116] W. L. Johnson, R. Busch, and U. Ko, "SYNTHESIS AND CHARACTERIZATION OF," vol. 47, no. 8, pp. 2455–2462, 1999.

[117] H. Choi-yim, R. D. Conner, F. Szuecs, and W. L. Johnson, "Processing, Microstructure, and Properties of Ductile Metal Particulate Reinforced Zr57Nb5Al10Cu15.4Ni12.6 Bulk Metallic Glass Composites," *Acta Mater.*, vol. 50, no. 10, pp. 2737–2745, 2002.

[118] H. Ma, J. Xu, and E. Ma, "Mg-based bulk metallic glass composites with plasticity and high strength," *Appl. Phys. Lett.*, vol. 83, no. 14, pp. 2793–2795, 2003.

[119] D. G. Pan, H. F. Zhang, A. M. Wang, and Z. Q. Hu, "Enhanced plasticity in Mg-based bulk metallic glass composite reinforced with ductile Nb particles," *Appl. Phys. Lett.*, vol. 89, no. 26, pp. 1–4, 2006.

[120] J. S. C. Jang, J. Y. Ciou, T. H. Hung, J. C. Huang, and X. H. Du, "Enhanced mechanical performance of Mg metallic glass with porous Mo particles," *Appl. Phys. Lett.*, vol. 92, no. 1, 2008.

[121] D. H. Bae, M. H. Lee, D. H. Kim, and D. J. Sordelet, “Plasticity in Ni59Zr20Ti16Si2Sn3metallic glass matrix composites containing brass fibers synthesized by warm extrusion of powders,” *Appl. Phys. Lett.*, vol. 83, no. 12, pp. 2312–2314, 2003.

[122] M. H. Lee, J. H. Kim, J. S. Park, J. C. Kim, W. T. Kim, and D. H. Kim, “Fabrication of Ni-Nb-Ta metallic glass reinforced Al-based alloy matrix composites by infiltration casting process,” *Scr. Mater.*, vol. 50, no. 11, pp. 1367–1371, 2004.

[123] J. E. Shield, M. J. Kramer, and I. Introduction, “Materials research,” pp. 2043–2047, 1997.

[124] C. Fan, R. T. Ott, and T. C. Hufnagel, “Metallic glass matrix composite with precipitated ductile reinforcement,” *Appl. Phys. Lett.*, vol. 81, no. 6, pp. 1020–1022, 2002.

[125] J. C. Tan, J. D. Furman, and A. K. Cheetham, “Relating Mechanical Properties and Chemical Bonding in an Inorganic - Organic Framework Material : A Single - Crystal Nanoindentation Study,” no. 100, pp. 14252–14254, 2009.

[126] C. M. Reddy, R. C. Gundakaram, S. Basavoju, M. T. Kirchner, K. A. Padmanabhan, and G. R. Desiraju, “Structural basis for bending of organic crystals,” *Chem. Commun.*, vol. 1, no. 31, p. 3945, 2005.

[127] C. Karunatilaka, D. K. Bučar, L. R. Ditzler, T. Friščić, D. C. Swenson, L. R. MacGillivray, and A. V. Tivanski, “Softening and hardening of macro- and nano-sized organic cocrystals in a single-crystal transformation,” *Angew. Chemie - Int. Ed.*, vol. 50, no. 37, pp. 8642–8646, 2011.

[128] S. Varughese, M. S. R. N. Kiran, U. Ramamurty, and G. R. Desiraju, “Nanoindentation in Crystal Engineering: Quantifying Mechanical Properties of Molecular Crystals,” *Angew. Chemie Int. Ed.*, vol. 52, no. 10, pp. 2701–2712, 2013.

[129] S. Varughese, M. S. R. N. Kiran, U. Ramamurty, and G. R. Desiraju, “Nanoindentation as a probe for mechanically-induced molecular migration in layered organic donor-acceptor complexes,” *Chem. - An Asian J.*, vol. 7, no. 9, pp. 2118–2125, 2012.

[130] V. Domnich, Y. Gogotsi, M. Trenary, and T. Tanaka, “Nanoindentation and Raman spectroscopy studies of boron carbide single crystals,” *Appl. Phys. Lett.*, vol. 81, no. 20, pp. 3783–3785, 2002.

[131] Y. Wang, D. Raabe, C. Klüber, and F. Roters, “Orientation dependence of nanoindentation pile-up patterns and of nanoindentation microtextures in copper single crystals,” *Acta Mater.*, vol. 52, no. 8, pp. 2229–2238, 2004.

[132] J. B. Ma and M. A. Zikry, “Nanoindentation and microstructural evolution of polycrystalline gold,” *J. Mater. Res.*, vol. 24, no. 3, pp. 1093–1104, 2009.

[133] A. Gouldstone, H. J. Koh, K. Y. Zeng, A. E. Giannakopoulos, and S. Suresh, “Discrete and continuous deformation during nanoindentation of thin films,” *Acta Mater.*, vol. 48, no. 9, pp. 2277–2295, 2000.

[134] Y. I. Golovin, V. I. Ivolgin, V. a Khonik, and K. Kitagawa, “Serrated plastic ¯ ow during nanoindentation of a bulk metallic glass,” *Scr. Mater.*, vol. 45, no. 8, pp. 947–952, 2001.

[135] B. Yang, L. Riester, and T. G. Nieh, “Strain hardening and recovery in a bulk metallic glass under nanoindentation,” vol. 54, pp. 1277–1280, 2006.

[136] W. C. Oliver, G. M. Pharr, and I. Introduction, “An improved technique for determining the gardness and elastic modulus using load and displacement sensing indentation experiments,” *J. Mater. Res.*, vol. 7, no. 6, p. 1564 to 1583, 1992.

[137] I. N. Sneddon, “The relation between load and penetration in the axisymmetric boussinesq problem for a punch of arbitrary profile,” *Int. J. Eng. Sci.*, vol. 3, no. 1, pp. 47–57, 1965.

[138] R. Limbach, K. Kosiba, S. Pauly, U. Kühn, and L. Wondraczek, “Serrated flow of CuZr-based bulk metallic glasses probed by nanoindentation: Role of the activation barrier, size and distribution of shear transformation zones,” *J. Non. Cryst. Solids*, vol. 459, pp. 130–141, 2017.

[139] R. Vaidyanathan, M. Dao, G. Ravichandran, and S. Suresh, “Study of mechanical deformation in bulk metallic glass through instrumented indentation,” *Acta Mater.*, vol. 49, no. 18, pp. 3781–3789, 2001.

[140] C. A. Schuh, T. G. Nieh, and Y. Kawamura, “Rate dependence of serrated flow during nanoindentation of a bulk metallic glass,” *J. Mater. Res.*, vol. 17, no. 7, pp. 1651–1654, 2002.

[141] G. Liao, Z. Long, M. Zhao, M. Zhong, W. Liu, and W. Chai, “Serrated flow behavior in a Pd-based bulk metallic glass under nanoindentation,” *J. Non. Cryst. Solids*, vol. 460, pp. 47–53, 2017.

[142] H. Guo, C. Jiang, B. Yang, and J. Wang, “Deformation behavior of Al-rich metallic glasses under nanoindentation,” *J. Mater. Sci. Technol.*, vol. 33, no. 11, pp. 1272–1277, 2017.

[143] R. S. and W. D. N. Wright, Wendelin J., “Deformation mechanisma of the Zr40Ti14Ni10Cu12Be24 bulk metallic glass,” *Mater. Trans.*, vol. 42, no. 4, p. 642 to 649, 2001.

[144] N. K. Mukhopadhyay and P. Paufler, “Micro- and nanoindentation techniques for mechanical characterisation of materials,” *Int. Mater. Rev.*, vol. 51, no. 4, pp. 209–245, 2006.

[145] Y. I. Golovin, Y. L. Iunin, and a. I. Tyurin, “Strain-rate sensitivity of the hardness of crystalline materials under dynamic nanoindentation,” *Dokl. Phys.*, vol. 48, no. 9, pp. 505–508, 2003.

[146] P. F. Yang, Y. S. Lai, S. R. Jian, J. Chen, and R. S. Chen, “Nanoindentation identifications of mechanical properties of Cu6Sn5, Cu3Sn, and Ni3Sn4intermetallic compounds derived by diffusion couples,” *Mater. Sci. Eng. A*, vol. 485, no. 1–2, pp. 305–310, 2008.

[147] T. Tsuru and Y. Shibutani, “Anisotropic effects in elastic and incipient plastic deformation under (001), (110), and (111) nanoindentation of Al and Cu,” *Phys. Rev. B - Condens. Matter Mater. Phys.*, vol. 75, no. 3, pp. 1–6, 2007.

[148] S. Tamimi, M. Ketabchi, N. Parvin, M. Sanjari, and A. Lopes, “Accumulative Roll Bonding of Pure Copper and IF Steel,” vol. 2014, 2014.

[149] J. S. Carpenter, S. C. Vogel, J. E. Ledonne, D. L. Hammon, I. J. Beyerlein, and N. A. Mara, "Bulk texture evolution of Cu-Nb nanolamellar composites during accumulative roll bonding," *Acta Mater.*, vol. 60, no. 4, pp. 1576–1586, 2012.

[150] S. Ohsaki, S. Kato, N. Tsuji, T. Ohkubo, and K. Hono, "Bulk mechanical alloying of Cu-Ag and Cu/Zr two-phase microstructures by accumulative roll-bonding process," *Acta Mater.*, vol. 55, no. 8, pp. 2885–2895, 2007.

[151] S. L. Semiatin and H. R. Piehler, "Formability of sandwich sheet materials in plane strain compression and rolling," *Metall. Trans. A*, vol. 10, no. 1, pp. 97–107, 1979.

[152] L. Ghalandari, M. M. Mahdavian, and M. Reihanian, "Microstructure evolution and mechanical properties of Cu/Zn multilayer processed by accumulative roll bonding (ARB)," *Mater. Sci. Eng. A*, vol. 593, pp. 145–152, 2014.

[153] J. M. Lee, B. R. Lee, and S. B. Kang, "Control of layer continuity in metallic multilayers produced by deformation synthesis method," *Mater. Sci. Eng. A*, vol. 406, no. 1–2, pp. 95–101, 2005.

[154] M. C. Chen, H. C. Hsieh, and W. Wu, "The evolution of microstructures and mechanical properties during accumulative roll bonding of Al/Mg composite," *J. Alloys Compd.*, vol. 416, no. 1–2, pp. 169–172, 2006.

[155] M. Stolpe, J. J. Kruzic, and R. Busch, "Evolution of shear bands, free volume and hardness during cold rolling of a Zr-based bulk metallic glass," *Acta Mater.*, vol. 64, pp. 231–240, 2014.

[156] C. Nagel, K. Rätzke, E. Schmidtke, F. Faupel, and W. Ulfert, "Positron-annihilation studies of free-volume changes in the bulk metallic glass Zr65Al7.5Ni10Cu17.5 during structural relaxation and at the glass transition," *Phys. Rev. B - Condens. Matter Mater. Phys.*, vol. 60, no. 13, pp. 9212–9215, 1999.

[157] W. H. Wang, R. J. Wang, W. T. Yang, B. C. Wei, P. Wen, D. Q. Zhao, and M. X. Pan, "Stability of ZrTiCuNiBe bulk metallic glass upon isothermal annealing near the glass transition temperature," *J. Mater. Res.*, vol. 17, no. 6, pp. 1385–1389, 2002.

[158] J. Gu, S. Ni, and S. Guo, "Effects of annealing on the hardness and elastic modulus of a Cu36Zr48Al8Ag8 bulk metallic glass," *Mater. Des.*, vol. 47, pp. 706–710, 2014.